이학석사 학위논문

리튬이차전지의 양극소재로써 고체전해질 LATP 및 탄소를 하이브리드 코팅한 $LiFe_{0.4}Mn_{0.6}PO_4$의 구조 및 전기화학적 특성 연구

Investigation of effects of
a hybrid Li-ion and electron conductive coating
on $LiFe_{0.4}Mn_{0.6}PO_4$ as a cathode material
for Li-ion batteries

울산대학교 대학원

화학과

김지민

Investigation of effects of a hybrid Li-ion and electron conductive coating on $LiFe_{0.4}Mn_{0.6}PO_4$ as a cathode material for Li-ion batteries

지도교수 이 영 일

이 논문을 이학석사학위 논문으로 제출함

2024 년 02 월

울산대학교 대학원

화학과

김지민

김지민의 석사학위 논문을 인준함

심사위원 이영일 (인)

심사위원 하지원 (인)

심사위원 이동호 (인)

울 산 대 학 교 대 학 원

2024 년 02 월

A hybrid Carbon-$Li_{1.3}Al_{0.3}Ti_{1.7}(PO_4)_3$ conductive coating for high current rate on $LiFePO_4$ cathode material

Chemical Engineering Journal

본 학위논문은 위 논문을 기반으로 하고 있음을 인준함

지도교수 이영일 (인)

English Abstract

The cathode material of a Lithium-ion battery (LIB) is the key material that determines the battery's energy and cycling performance. Encouraged by the successful commercialization of $LiFePO_4$ for electric vehicles (EVs), a combination of $LiFePO_4$ and $LiMnPO_4$ to form a $LiFe_xMn_{1-x}PO_4$ (LFMP) solid solution has attracted worldwide attention to combine the characteristics of the increase in conductivity brought by Fe and the higher energy density brought by Mn. However, its inherent low electron conductivity and Li-ion diffusion coefficient are critical obstacles to overcome. In this study, we proposed that a hybrid coating of Li-ion and electron conducting layers on the LFMP particle surface can simultaneously provide transfer paths for electrons and Li-ions to practically improve the overall performance of the LFMP material. To demonstrate our proposal, a conductive coating layer containing carbon (C) and $Li_{1.3}Al_{0.3}Ti_{1.7}(PO_4)_3$ (LATP) solid electrolyte on $LiFe_{0.4}Mn_{0.6}PO_4$ (LFMP) cathode material (LFMP@C_LATP) was successfully synthesized by the conventional solid-state method. The structure and morphology of LFMP@C_LATP were characterized by X-ray diffraction and a scanning electron microscope equipped with energy dispersive X-ray spectroscopy. Solid-state nuclear magnetic resonance with the magic angle spinning technique identified the formation of LATP while thermogravimetric analysis and Raman spectroscopy measurements characterized the carbon layer. The electrochemical properties were studied by cyclic voltammetry, electrochemical impedance spectroscopy, and galvanostatic intermittent titration technique. Our systematic investigation revealed that the LFMP@C_LATP exhibits excellent capacity and cycling performance, compared to the pristine LFMP and the conventional carbon-coated LFMP (LFMP@C). Considering the effects of the coating, the hybrid coating material was found to improve

the Li-ion diffusivity, prolong and stabilize the operating voltage of the core LFMP, and contribute an additional capacity to the LFMP material.

국문 초록

리튬이온 배터리의 양극 소재는 배터리 에너지를 결정하는 핵심 소재다. 전기자동차용(EV)용 리튬인산철 ($LiFePO_4$, LFP)의 성공적인 상용화에 힘입어, 리튬인산철의 상대적으로 높은 전도 특성과 리튬인산망간 ($LiMnPO_4$, LMP)의 높은 에너지 밀도 특성을 결합한 리튬인산철망간 ($LiFe_xMn_{1-x}PO_4$, LMF)이 전세계적으로 많은 주목을 받고 있다. 그러나 LFMP 는 본질적으로 낮은 전자전도도와 리튬이온확산계수를 가지고 있다. 따라서, LFMP 표면에 리튬이온 및 전자전도층을 하이브리드 코팅함으로써 전자와 리튬이온의 전달경로를 동시에 제공하며 단점을 극복할 수 있을 것으로 기대된다. 본 연구에서는 탄소 (C)와 $Li_{1.3}Al_{0.3}Ti_{1.7}(PO_4)_3$ (LATP) 고체 전해질을 하이브리드 코팅한 LFMP (LFMP@C_LATP)를 고상법으로 합성했다. LFMP@C_LATP 의 구조 및 형태를 분석하기 위해 X-선 회절 장치(XRD), 에너지 분산형 X-선 분광기(EDS)가 장착된 주사 전자 현미경(SEM)을 이용한다. MAS 기법을 이용한 solid state NMR 을 통해 LFMP 표면의 리튬이온전도층인 LATP 를 확인했으며, 열중량분석(TGA) 및 라만 분광기(Raman)를 측정함으로써 탄소층을 조사했다. 전기화학적 성능은 galvanostatic automatic battery cycler 를 이용한 충·방전 테스트 및 전기화학 임피던스 분광법 (EIS), 정전류식 간헐적적정 테크닉 (GITT) 측정 통해 평가되었다. 그 결과, LFMP@C_LATP 는 pristine LFMP 와 LFMP@C 에 비해 우수한 용량 및 사이클링 성능을 나타냈다. 하이브리드 코팅층은 리튬이온 확산도를 개선하고 전압 고원을 연장 및 안정화하며 LFMP 에 추가적인 용량을 기여하는 것을 확인할 수 있었다.

Contents

English Abstract **5**

국문 초록 **7**

List of Tables **10**

List of Figures **11**

1. Introduction **13**

1.1 Principle of Li-ion batteries 16

1.2 Cathode materials for Li-ion batteries 20

1.2.1 Features of cathode materials 20

1.2.2 Material structure and electrochemical properties 24

1.3 Development of $LiFe_{1-x}Mn_xPO_4$ cathode materials 28

2. Experimental **31**

2.1 Material synthesis 31

2.2 Material characterization 33

2.3 Electrochemical performance 34

3. Results and Discussion **36**

3.1 Material characterization 36

3.1.1 X-ray diffraction 36

3.1.2 ^{7}Li and ^{31}P magic angle spinning nuclear magnetic resonance 38

3.1.3 Raman spectroscopy and Thermal gravimetric analysis 41

3.1.4 Field emission scanning electron microscopy and energy dispersive x-ray spectroscopy 43

3.2 Electrochemical performance 45

3.2.1 Cyclic voltammetry 45

3.2.2 Electrochemical impedance spectroscopy 52

3.2.3 Galvanostatic intermittent titration technique 48

3.2.4 Cycling performance 52

4. Conclusion 63

5. Reference 65

List of Tables

Table 1.1. The properties of typical cathode active materials.[17]

Table 1.2. Scheme of the cell configuration and electrochemical charging and discharging process of lithium-ion battery.[6]

Table 3.1. Slope and intercept of the relationship between the resistance (Re(Z)) and the inverse square root of the angular frequency ($\omega^{-1/2}$) of pristine LFMP, LFMP@C, and LFMP@C_LATP.

Table 3.2. Discharge capacity for the 1st and 50th cycles and capacity retention rates of pristine LFMP, LFMP@C, and LFMP@C_LATP.

Table. 3.3. Summary of long cycle performance of pristine LFMP, LFMP@C, and LFMP@C_LATP at 1.0 C.

List of Figures

Fig. 1.1. Comparison of various secondary batteries.[3]

Fig. 1.2. Scheme of the cell configuration and electrochemical processes of a LIB.[7]

Fig. 1.3. Crystal structure of the three lithium-insertion compounds in which the Li ions are mobile through the 2-D (layered), 3-D (spinel), and 1-D (olivine) frameworks.[18]

Fig. 2.1. Solid-state synthetic procedures of LFMP@C_LATP.

Fig. 1.3. Crystal structure of the three lithium-insertion compounds in which the Li+ ions are mobile through the 2-D (layered), 3-D (spinel), and 1-D (olivine) frameworks. Battery.[17]

Fig. 1.4. Typical technical solutions to improve the olivine cathodes, including morphology control,[42] element doping[43], and surface coating.[44]

Fig. 2.1. Solid-state synthetic procedure of LFMP@C_LATP.

Fig. 2.2 Schematic diagram of the coin cell fabrication for electrochemical investigation.

Fig. 3.1. (a) The XRD patterns of pristine LFMP, LFMP@C, LFMP@C_LATP and (b) LATP synthesized at the same conditions.

Fig. 3.3. (a) ^{7}Li and (b) ^{31}P MAS NMR spectra of LATP synthesized under the coating conditions. The isotropic peaks are marked with asterisks.

Fig. 3.4. (a) Raman spectra and (b) TGA curves of LFMP@C and LFMP@C_LATP.

Fig. 3.5. (a) SEM image and (d) EDS layer image of LFMP@C_LATP with corresponding elemental distribution (b) Fe, (c) Mn, (e) Ti, and (f) C.

Fig. 3.6. (a) CV profiles of pristine LFMP, LFMP@C, and LFMP@C_LATP. (b) CV profile of LATP prepared under the conditions for coating.

Fig. 3.7. (a) GITT profiles and (b) typical charge-rest and discharge-rest pulses of LFMP@C and LFMP@C_LATP. The cells are constantly charged or discharged at 0.05 C for 15 min, followed by relaxation for 1h in the voltage range of 2.0-4.5 V, vs. Li/Li^+.

Fig. 3.8. (a) Nyquist plots and (b) the linear relationship between Re(Z) and $\omega^{-1/2}$ of pristine LFMP, LFMP@C and LFMP@C_LATP. The linear relationship is calculated in the low-frequency range of 100 mHz to 1 Hz.

Fig. 3.9. (a) Rate performance at various C-rates from 0.05 C to 5.0 C and (b) typical charge-discharge profiles of pristine LFMP, LFMP@C and LFMP@C_LATP at 0.05 C.

Fig. 3.10. Long cycle performance of pristine LFMP, LFMP@C, and LFMP@C_LATP at 1.0 C.

1. Introduction

A battery is a device that converts chemical energy into electrical energy through spontaneous oxidation-reduction reactions. Batteries can be divided into primary and secondary batteries. Primary batteries include alkaline batteries, zinc-carbon (Zn-C) batteries, lithium (Li) batteries, etc.[1] The electrochemical reaction in primary batteries is irreversible, which means that once their chemical energy is depleted, they cannot be recharged and reused. Therefore, primary batteries can only be used once in their lifetime. They are typically used in low-drain devices such as remote controls, flashlights, and some medical devices. In contrast, secondary batteries can be recharged and reused many times, making them more cost-effective and environmentally friendly in the long run. Secondary batteries include nickel metal hybrid batteries (NiMH), nickel-cadmium batteries (NiCd), lithium-ion batteries (Li-ion), etc.[2] They are commonly used in high-drain devices such as laptops, smartphones, electric vehicles, and renewable energy storage systems. The choice between primary and secondary batteries depends on the requirements of the specific application, such as energy density, cost, environmental impact, and the need for reusability.

Lithium-ion batteries (LIBs) are a type of rechargeable battery that has gained widespread popularity due to their high energy density, relatively low self-discharge, and ability to be recharged hundreds of times. A LIB stores and uses lithium ions as its main energy source. Lithium is the lightest metal and has the lowest standard reduction potential, allowing high electromotive forces of over 3V to be achieved, resulting in high energy and power density when used as an electrode material, as shown in **Fig.1.1**.[3]. In addition, LIBs have a wide operating temperature range, fast charging capability, no memory effect, relatively long cycle life, and low self-discharge

rate.[4] For these reasons, LIBs are widely used in mobile applications such as cell phones and laptops and dominate the electric vehicle (EV) and energy storage system (ESS) markets.

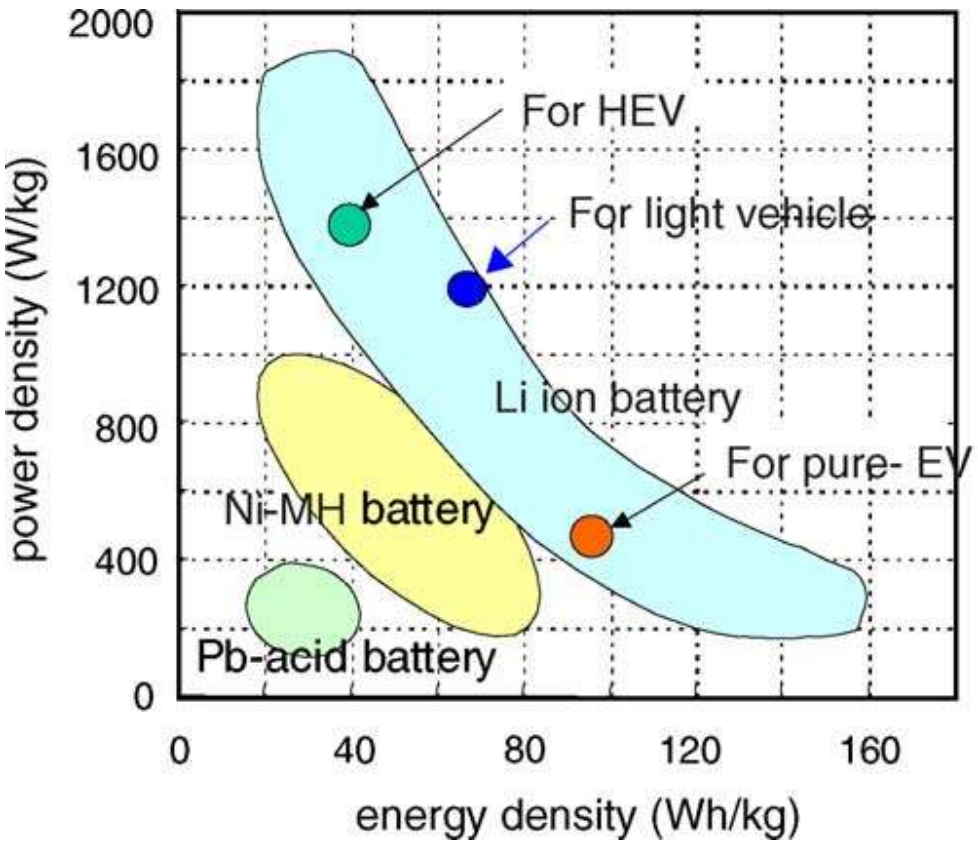

Fig. 1.1. Comparison of different secondary batteries.[3]

1.1 Principle of Li-ion batteries

Li-ion rechargeable batteries consist of two electrodes, anode and cathode, immersed in an electrolyte and separated by a polymer membrane. This basic device configuration has remained throughout the development of the batteries. The anode and cathode of a typical Li-ion battery (LIB) have different potentials, resulting in a potential difference. The potential difference is the electromotive force that facilitates the movement of Li ions between the two electrodes and induces the flow of electricity in an electric circuit. During charging, an external power source provides a voltage that drives the Li ions from the positive electrode (cathode) through the electrolyte to the negative electrode (anode). The Li ions are embedded or intercalated into the structure of the host material in the anode, typically made of graphite or other carbon-based materials. Simultaneously, the cathode material releases the Li ions and electrons. When the battery is discharged, an electrochemical oxidation reaction occurs at the anode. The Li ions are de-intercalated from the anode, transferred through the electrolyte, and react with the host material in the cathode. The movement of the Li ions results in the flow of electrons through the external circuit, generating an electric current that powers the connected devices. The heterogeneous redox reactions in LIBs are always accompanied by solid-state mass diffusion and the Li-ion concentration varies in the cathode and anode with the charge and discharge states. The electrochemical reactions during the charge/discharge of a LIB consisting of a $LiFePO_4$ cathode and a conventional carbon anode are shown below.

At the cathode $xLi^+ + xe^- + Li_{1-x}FePO_4 \leftrightarrow LiFePO_4$

At the anode $Li_xC_6 \leftrightarrow xLi^+ + xe^- + C_6$

Overall reaction $LiFePO_4 \leftrightarrow FePO_4 + LiC_6$

The process of charging and discharging a lithium-ion battery is shown in **Fig.1.2**. The electrolyte is a Li-ion conductor and is not conductive to electrons. The electrode and electrolyte must be in contact to allow Li ions to be transferred. The anode and cathode should be in close contact to minimize internal resistance but their direct contact will cause an internal short circuit, and thus a separator must be placed between these two electrodes to prevent this.[5] In a LIB, both electrodes have current collectors that help transport electrons. Cu foil is usually used as the current collector for the anode while Ai foil is used for the cathode. In addition to the active materials, the electrodes contain polymeric binders to bind the active material particles together, and carbon black to enhance electron conductivity.

The cell voltage strongly depends on the compatibility of the cathode, anode, and electrolyte.[6] The cell working voltage is generally determined based on the difference in chemical potential between the anode and the cathode. This working voltage is limited by the electrochemical window of the electrolyte which is determined by the energy gap from the highest occupied molecular orbital (HOMO) to the lowest unoccupied molecular orbital (LUMO). The anode and cathode must be carefully selected. While the potential of the anode is below the LUMO, the potential of the cathode is located above the HOMO to prevent the reduction of the electrolyte on the anode and the oxidation of the electrolyte on the cathode. The electrolyte redox reactions induce the formation of a passivating solid electrolyte interphase film which leads to both power and capacity loss.

The charge-discharge process is reversible, allowing the battery to be charged and discharged multiple times. The efficiency and performance of the battery are affected by factors such as the rate of charge and discharge, temperature, and the nature of materials used in the electrodes and

electrolyte. Understanding these factors is essential but challenging for optimizing the performance, longevity, and safety of LIBs in various applications.

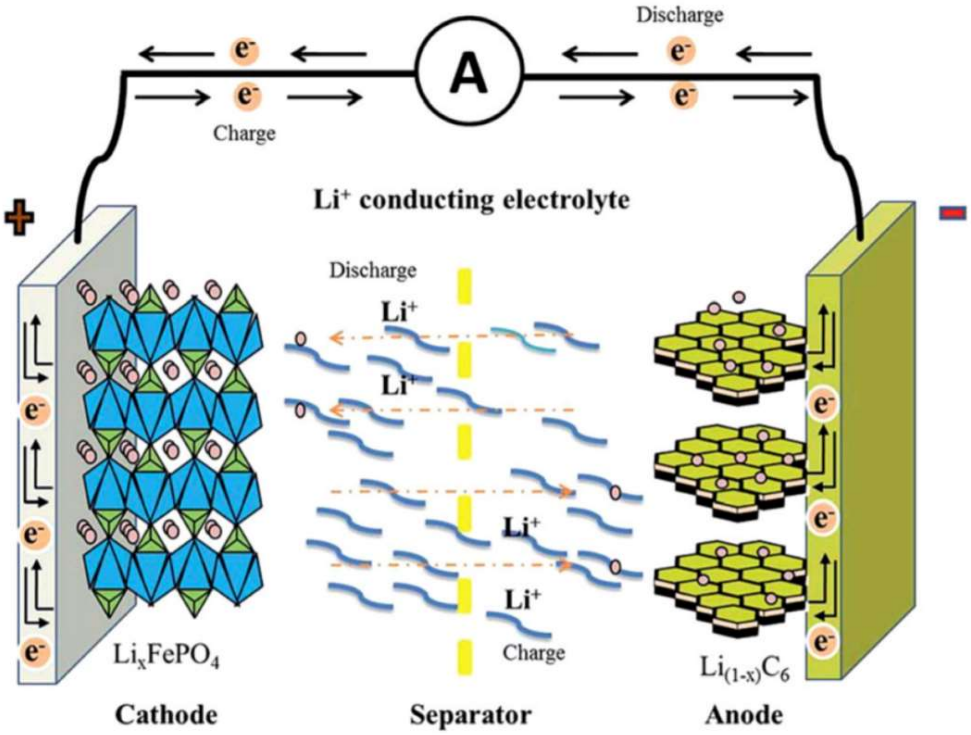

Fig. 1.2. Scheme of the cell configuration and electrochemical processes of a LIB.[7]

1.2 Cathode materials for Li-ion batteries

1.2.1 Features of cathode materials

Cathode materials are a critical component of LIBs and play a key role in determining the battery's performance, capacity, and voltage since they are responsible for storing and releasing Li-ions during the charge and discharge cycles. In addition, almost half the cost of battery manufacturing is related to the processing of the cathode material.[8,9] When cycling, Li ions are transferred back and forth between the anode and the cathode through the electrolyte. The Li-ion intercalation must be easy and the structure of the active material must remain stable.[10] Any irreversible phase transitions in the crystalline structure of the host materials will reduce the capacity delivery and shorten the battery lifetime, thus it must be critically avoided.[12,13,14] To achieve high power, the cathode material must be as light as possible and must possess high electronic and ionic conductivity.[15] Additionally, the cathode material must be electrochemically stable and comparable to the electrolyte to prevent unexpected reactions that may reduce its efficiency.[15, 16]

Several selection criteria for cathode materials for LIBs have been proposed, considering their impacts on society, economy, and techniques. A potential cathode material should possess natural abundance, eco-friendly characteristics for processing, usage, and recycling, and, especially, low cost. The electrode materials must offer a large reversible storage capacity and high energy density. Cathode materials are commonly transition metal compounds, oxides, or complex oxides. Typical commercialized cathode materials include layered oxides $LiMO_2$ (M = Co, Ni, Mn), spinel oxides LiM_2O_4 (M = Mn, Ni), and olivine $LiMPO_4$ (M = Fe, Mn, Co, Ni). The properties of these typical

cathode materials are listed in **Table 1.1** and their crystal structures are shown in **Fig. 1.3**. Detailed discussion of their performance is given in the following section.

Table 1.1. The properties of some typical cathode materials.[17]

Properties	$LiCoO_2$	$LiNiO_2$	$LiMn_2O_4$	$LiFePO_4$
Redox couple	Co^{4+}/Co^{3+}	Ni^{4+}/Ni^{3+}	Mn^{4+}/Mn^{3+}	Fe^{3+}/Fe^{2+}
Voltage (V)	3.6	4.0	3.9	3.5
Specific capacity (mAh g^{-1})[a]	274	274	148	170
Discharge capacity (mAh g^{-1})[a]	145	160	105	155
Eco-friendliness	Poor	Fair	Good	Good
Availability	Low	Fair	High	High
Cost	High	Fair	Low	Low

[(a)] Theoretical, [(b)] Practical

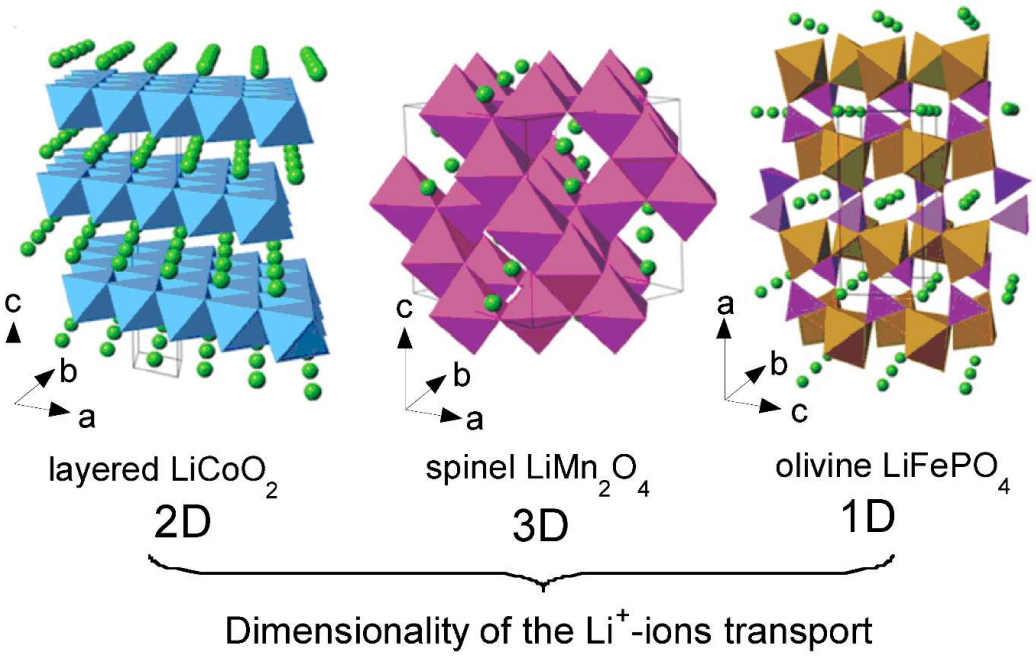

Fig. 1.3. Crystal structure of three common cathode compounds. In their structures, Li ions are mobile through the 2-D (layered $LiCoO_2$), 3-D (spinel $LiMn_2O_4$), and 1-D (olivine $LiFePO_4$) frameworks.[18]

1.2.2 Material structure and electrochemical properties

Layered oxides ($LiMO_2$ with M = Co, Mn, Ni) have been the most widely used and commercialized cathode materials for LIBs.[19,20] The structure of lithium transition metal oxide is shown in **Fig.1.3**. $LiCoO_2$ is the parent compound of this $LiMO_2$ family, which was first suggested as the intercalation compound for rechargeable LIBs in 1976 and then commercialized in the early 1990s. $LiMO_2$ is densely packed with slabs of edge-sharing MO_6 octahedra separated by interstitial layers of Li.[21] In this structure, relatively large amounts of Li ions can be stored between the wide, flat layers. More importantly, the Li-ions can easily move through its two-dimensional channels.[22] However, with the Li-ion removal from the layered crystal lattice during charging, nonstoichiometric $Li_{1-x}CoO_2$ compounds are formed. An irreversible crystal transformation occurs when half of the Li ions have been extracted from the parent structure, resulting in a practically achievable capacity of 145 mAh g^{-1} (**Table 1.1**). Due to this low practical capacity and the relatively high cost of Co, a layered $LiNiO_2$ has been developed as a possible replacement (**Table 1.1**). However, extensive characterizations have revealed the presence of the Li-Ni disorder due to the very similar ionic radii of Li^+ and Ni^{2+}. Furthermore, Ni-rich layered oxides, $LiNi_{1-x-y}Co_xM_yO_2$ with M = Mn, Al, etc. known as NCM, NCA, which possess high specific capacity depending on Ni fraction, become the most widely used cathode materials for high-energy-density LIBs. Recently, industrialization and commercialization of Co-free Ni-rich cathode materials have been pursued. [23,24]

LiM_2O_4 (LiM_2O_4, M = Mn, Ni) is a class of cathode material with a spinel structure. $LiMn_2O_4$ was first proposed for LIBs in the early 1980s. LiM_2O_4 is highly stable because of the strong edge-sharing of octahedral MO_6 to form a lattice structure.[25] Moreover, the unique crystal framework

allows Li ions to diffuse through three-dimensional channels (**Fig.1.3**) and is therefore very promising for high-energy and high-power applications.[26] The 3D diffusion path can provide excellent rate capability. In addition, the large amount of Mn can guarantee good thermal stability. However, its limited practical discharge capacity results in limited achievable energy density despite the rather high operating voltage (**Table 1.1**). Moreover, it suffers from severe capacity fading, especially when cycling at elevated temperatures, due to the irreversible structural transformation caused by the presence of Jahn-Teller (J-T) active Mn^{3+} ions and the dissolution of Mn^{2+} in the electrolyte by the corrosion of H^+.[27,28] Adding Ni to $LiMn_2O_4$ increases its cyclability but causes electrolyte decomposition on the particle surface due to the high potential of the Ni^{2+}/Ni^{4+} redox couple.

The olivine-based cathode materials $LiMPO_4$ (M = Mn, Fe, Co, Ni) with a successful commercialization of $LiFePO_4$ (LFP) have been extensively studied.[29,30] In particular, LFP attracts a lot of attention due to its inherited merits, including relatively high specific capacity, low cost, abundant availability, low toxicity, and high safety, as shown in **Table 1.1**.[31] The crystal structure of fully discharged $LiFePO_4$ and fully charged state $FePO_4$ is similar, and thus a small volume change occurs during cycling, leading to an excellent cycle life and low capacity fade.[32] However, LFP exhibits the disadvantage of a low Li-ion diffusion coefficient and low electron conductivity, as Li-ion transport occurs by diffusion through one-dimensional channels (**Fig.1.3**)[33], thus its high current charging and discharging capacity are crucially limited. LFP cathode has a lower operating voltage and thus a lower energy density than other olivine phosphate materials such as $LiMnPO_4$ (LMP), $LiCoPO_4$ (LCP), and $LiNiPO_4$ (LNP). As a result, the LMP, LCP, LNP, and their combinations have attracted considerable effort for high-voltage olivine cathodes. Unfortunately,

their intrinsic characteristics of lower conductivity and higher resistivity than the LFP limit their practical performance. In addition, LMP is electrochemically inactive and suffers from structural distortion and the discharge voltage plateaus of LCP and LNP are outside the potential window of the common electrolytes to be pessimistically suitable for Li-ion batteries.[34] To practically improve the performance of the olivine materials, studies have been strongly focusing on morphology control,[35,36] doping,[37,38] and coating the particles to increase both electron conductivity and Li-ion diffusivity (**Fig 1.4**).[39,40] While morphology control and ion doping aim to facilitate Li-ion transfer in the crystal structure, the surface coating can improve the overall conductivity of the material and protect the particle surface from unexpected interfacial reactions. As an effective strategy to modify the interfacial chemistry of electrode materials, surface coating has become a leading strategy to improve the overall electrochemical performances of the olivine cathode material. It should be emphasized that carbon coating is the most common approach for olivine materials. Carbon can be deposited *in situ* on the particle surface during synthesis and can simultaneously reduce particle size, improve conductivity, and enhance structural and thermal stabilities. The quality of the carbon coating generally depends on the carbon source and the synthetic conditions. However, as the electron conductivity can be remarkably improved by the carbon coating, the Li-ion diffusion can be the rate-limiting factor and thus the Li-ion conductive coating is vital to regulate the Li-ion migration at the interfaces. Results from Kang et al.[41] showed that nanosized LFP with pyrophosphate coating provided a capacity of 130 mAh g^{-1} at 50.0 C. Their research provided experimental evidence for the need for a Li-ion conductive coating material on the LFP particle surface for practical improvement.

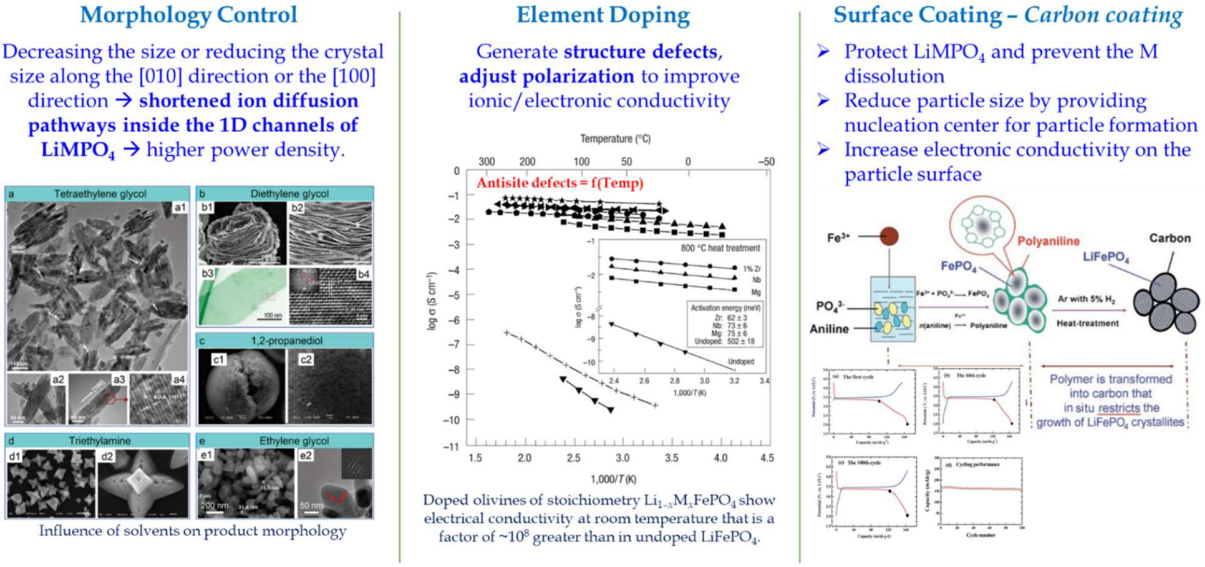

Fig. 1.4. Typical technical solutions to improve the olivine cathodes, including morphology control,[42] element doping[43], and surface coating.[44]

1.3 Development of $LiFe_{1-x}Mn_xPO_4$ cathode materials

Encouraged by the successful commercialization of $LiFePO_4$, various combinations of transition metals (M = Mn, Fe, Co, Ni) have been studied to develop multicomponent olivine materials with higher energy density to broaden their applications.[45,46,47,48] This approach has been demonstrated by the mature development of $LiFe_xMn_{1-x}PO_4$ (LFMP) and the involvement of Co in the formation of $LiFe_xMn_yCo_{1-x-y}PO_4$ (LFMCP). With a negligible difference in the ionic radii of Fe^{2+} and Mn^{2+}, the LFMP is a stable solid solution for a wide range of Fe:Mn ratio with a critical composition of Mn of 0.8 to preserve the same crystal phase during cycling.[49] The solid solution LFMP is of interest to take advantage of both Fe and Mn to achieve the increase of conductivity brought by Fe, and the higher energy density brought by Mn. The delithiated Fe-rich domains can promote a more effective local structural change and thus facilitate the delithiation of the neighboring Mn-rich domains.[50] The coexistence of Fe and Mn on the transition metal sites, therefore, results in higher apparent diffusivity values with respect to Mn as compared to $LiMnPO_4$. However, the Li-ion diffusivity values in the Mn regime are remarkably lower than those in the Fe regime, making Mn to be the rate-limiting factor in the Mn-containing olivine materials. In addition, the strong electron-lattice interaction induced by the trivalent manganese (Mn^{3+}:$3d^4$) in the charged state ($Fe_x^{3+}Mn_{1-x}^{3+}$)PO_4 has been highlighted as the intrinsic obstacle, leading to large anisotropic distortion and structural destabilization. As a result, it has been critical to achieving full theoretical capacity and high capacity retention for LFMP materials. In addition, the delithiation of the LFMP is prevented and the degradation is induced by the spin-transition of Mn^{3+} from the high-spin to the low-spin state with the critical Fe:Mn ratio of 0.4:0.6 and thus the decent electrochemical properties of the LFMP have been proposed in the Mn range of less than 0.6 at

slow rates.[51] Controlling particle size,[52,53] doping,[54,55, 56] and surface modification[57,58] have been studied to improve both electron and Li-ion conductivity. However, the carbon coating layer can block the insertion/extraction of lithium ions by increasing the activation barrier for lithium-ion migration at the interface.[59,60] Therefore, it is necessary to balance electron conduction and lithium-ion diffusion.[61] Most available Li-ion conductors for coating rely on a solid electrolyte. A solid electrolyte coating improves the charge transfer at the cathode-electrolyte interface and provides a physical barrier to protect the cathode material from undesirable side reactions. Among common solid electrolytes, the phosphate-based NASICON–type $Li_{1.3}Al_{0.3}Ti_{1.7}(PO_4)_3$ (LATP) is attractive to be employed due to its high ionic conductivity at room temperature and good chemical stability in the ambient atmosphere. In addition, the LATP is compatible and stable with olivine materials. The sintered product from a mixture of LFP and LATP can form a small fraction of NASICON–type $Li_2FeTi(PO4)_3$ interphase,[62] which exhibits comparable ionic conductivity with that of LATP and significantly enhances Li ion transport kinetics within bulk LFP during charge and discharge processes.

In this study, the benefit of the interfacial Li-ion transfer channels for practical improvement of a high-voltage $LiFe_{0.4}Mn_{0.6}PO_4$ (LFMP) olivine cathode has been investigated by comparing the electrochemical performance of three different materials, including pristine LFMP, carbon-coated LFMP (LFMP@C), and a combination of carbon and $Li_{1.3}Al_{0.3}Ti_{1.7}(PO_4)_3$ (LATP)-coated LFMP (LFMP@C_LATP). Different methods, including X-ray diffraction, ^{7}Li and ^{31}P magic angle spinning nuclear magnetic resonance measurements, and high-resolution transmission electron microscopy, have been used to characterize the crystal phase, structure, and morphology of the synthesized materials. The electrochemical characterizations by cyclic voltammetry,

electrochemical impedance spectroscopy, galvanostatic intermittent titration technique, and cycling performance have been performed to realize the advantages of the coating.

2. Experimental

2.1 Material synthesis

Hybrid coating of carbon (C) and $L_{1.3}A_{0.3}Ti_{1.7}(PO_4)_3$ (LATP) solid electrolyte on $LiFe_{0.4}Mn_{0.6}PO_4$ (LFMP) particles (LFMP@C_LATP) was synthesized by a two-step solid-state reaction in which pristine LFMP is first synthesized, followed by simultaneous coating of C and LATP as shown in **Fig 2.1**.

The $LiFe_{0.4}Mn_{0.6}PO_4$ (LFMP) and $L_{1.3}A_{0.3}Ti_{1.7}(PO_4)_3$ (LATP) precursors were separately prepared by mixing a stoichiometric amount of the corresponding raw materials in an acetone medium (Samchun, 99.7%) using a planetary mill (Pulverisette, Fritsch) with zirconia balls (ø = 5 mm, SciLab) at a speed of 300 rpm for 3 h. Li_2CO_3 (Aldrich, 99.0%), $FeC_2O_4.2H_2O$ (Junsei, 99.0%), $MnC_2O_4.2H_2O$ (Alfa Aesar, 99.0%), and $NH_4H_2PO_4$ (Junsei, 99.5%) were used to prepare LFMCP precursor, while Li_2CO_3, $AlOH(OOCCH_3)_2$ (Aldrich, 100.0%), TiO_2 (Aldrich, 100.0%), and $NH_4H_2PO_4$ were used to prepare LATP precursor. Sucrose (Junsei, 100%) was ground before use as the carbon source.

First, the prepared LFMP precursor was purged in the tube furnace under pure Ar gas at 170 °C for 3 h. It was then heated at 370 °C for 4 h and sintered at 670 °C for 6 h for the formation of pristine LFMP. LFMP@C and LFMP@C_LATP were synthesized by adding 7.5 wt% of sucrose or 7.5 wt% each of sucrose and LATP precursor to the synthesized pristine LFMP, followed by ball milling and heating in a tube furnace under the same conditions as before. LATP was synthesized under the conditions used for coating to evaluate the formation of the LATP solid electrolyte in this research.

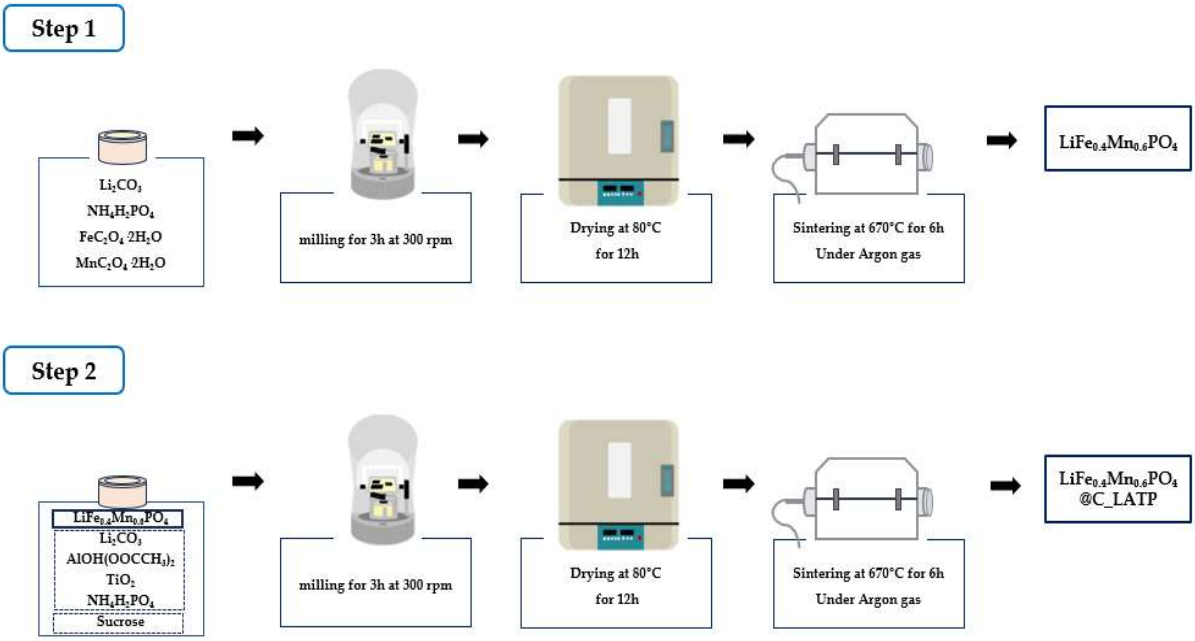

Fig. 2.1. Solid-state synthetic procedure of LFMP@C_LATP.

2.2 Material characterization

The powder X-ray diffraction (XRD) analysis was obtained using an X-ray diffractometer (Rigaku Ultima IV, Germany) with Cu K_α radiation (λ = 1.506) over a 2θ range between 10° and 80° in continuous scan mode at a rate of 2° min^{-1}. ^{7}Li and ^{31}P magic angle spinning (MAS) nuclear magnetic resonance (NMR, Bruker Avance III 300, Germany) measurements were performed at room temperature using a 7.04T magnet. The ^{7}Li NMR experiment was performed with a 2.5 mm MAS probe and the ^{31}P NMR experiments were performed with a 4.0 mm MAS probe. All spectra were observed with the Hanh-echo pulse sequence (90°–τ–180°–τ–acq), where $\tau = 1/\nu_r$. The ^{7}Li NMR spectra were referenced to a 1M LiCl at 0 ppm. The sample spinning rate was 27 KHz. All ^{7}Li MAS NMR spectra were acquired with a $\pi/2$ pulse width of 2.0 μs, a repetition delay of 0.5s, 512 transients, and a spectral width of 1.48MHz. The ^{31}P NMR spectra were referenced to $NH_4H_2PO_4$ at 0ppm. The sample spin rate was 13 KHz. All ^{31}P MAS NMR spectra were acquired with a $\pi/2$ pulse width of 4 μs, a repetition delay of 0.5 s, and 2048 transients. The ^{31}P NMR experiment was performed in two parts. One part of the signals could be obtained with the center of the chemical shift axis of 0ppm and the spectral width of 0.24 MHz. The other part of the signals could be obtained with the center of the chemical shift axis of 5000 ppm and the spectral width of 0.88 MHz. Thermogravimetric analysis was performed in air from room temperature to 750 °C at a heating rate of 10 °C min^{-1} using an SDT Q600 instrument. The Raman spectroscopy was performed with the use of a DXR™3 instrument (Thermo Fisher Scientific Inc., USA). The morphology and elemental composition of LFMP@C_LATP were investigated by field-emission scanning electron microscopy (FE-SEM, JEOLJSM-6500F, Japan) equipped with energy dispersive X-ray spectroscopy (EDX, Oxford Instrument X-Max, UK).

2.3 Electrochemical performance

The electrode was fabricated from a slurry containing 80 wt% synthesized active materials, 10 wt% Super P, and 10 wt% poly(vinylidene fluoride) (Aldrich, M_W = 534,000) in N-methyl-2-pyrrolidone (Duksan, HPLC grade) solvent. The electrochemical performances were measured using CR2032-type coin cells assembled in an Ar-filled glove box with a Li metal foil as the counter electrode, 1.0 M $LiPF_6$ in ethylene carbonate/dimethyl carbonate (EC:DMC = 1:1 v/v) as the electrolyte (Panax Etec Co. Ltd, Korea), and a porous polypropylene membrane (Celgard 2500) as the separator. The electrochemical impedance spectroscopy (EIS) measurements were performed at the same state of charge for all samples, using the SP-300 instrument (Biologic) in the frequency range of 100 mHz to 1 MHz. The galvanostatic intermittent titration technique (GITT) measurements were performed at 0.05 C with intermittent charging and discharging for 15 min followed by 1 h of rest in the voltage range of 2.0-4.5 V (vs. Li/Li^+). The cycling performance was tested using a Galvanostatic automatic battery cycler (WonATech WBCS 3000, Korea) with a constant current-constant voltage (CC-CV) protocol at various current rates (1.0 C = 170 mA g^{-1}) at room temperature.

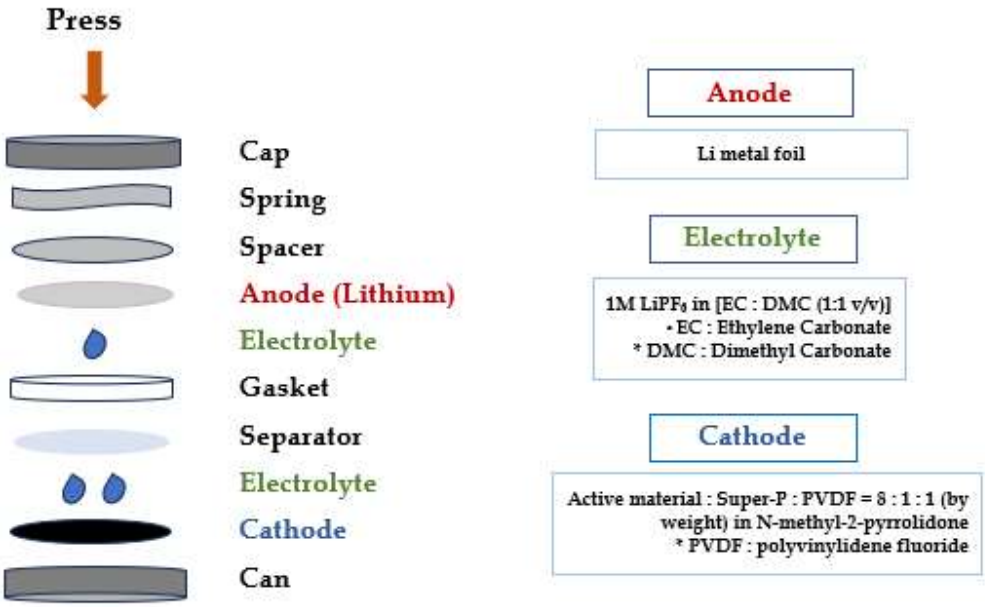

Fig. 2.2 Schematic diagram of the coin cell fabrication for electrochemical investigation.

3. Results and Discussion

3.1 Material characterization

3.1.1 X-ray diffraction

Fig. 3.1(a) shows the XRD patterns of pristine $LiFe_{0.4}Mn_{0.6}PO_4$ (LFMP), carbon-coated LFMP (LFMP@C), and carbon (C)- and $Li_{1.3}Al_{0.3}Ti_{1.7}(PO_4)_3$ (LATP)-coated LFMP (LFMP@C_LATP). The sharp diffraction peaks of all synthesized materials are well aligned and similar to the theoretical crystal peaks of olivine materials with *Pnma* space group. The well-matched XRD patterns between all three samples indicate that the LFMP material retains its structural integrity after coating. For LFMP@C and LFMP@C_LATP no peak of carbon can be identified. This is due to the small amount of carbon formed or the dominance of amorphous carbon. It is challenging to distinguish the crystal phase of the LATP after coating even though only the XRD pattern of LFMP@C_LATP shows the presence of minor peaks at the 2θ of 24.6° which are close to the most intense characteristic peak of LATP prepared under similar conditions (**Fig 3.1(b)**). As indicated in **Fig. 3.1(b)**, all XRD peaks of the synthesized LATP are well matched with the reference material (ICSD#14585), indicating that the synthesis conditions are suitable for forming LATP and, thus, for coating LATP on the LFMP particle surface. Some minor peaks corresponding to $AlPO_4$, Li_3PO_4, and TiO_2 are observed for the synthesized LATP. It should be noted that $AlPO_4$, Li_3PO_4, and TiO_2 have been used to coate on various LIB cathode materials, showing improvement in their practical performances.[65,66] Those minor phases with negligible fractions are not expected to contribute dramatically to the overall electrochemical characteristics of the coated materials.

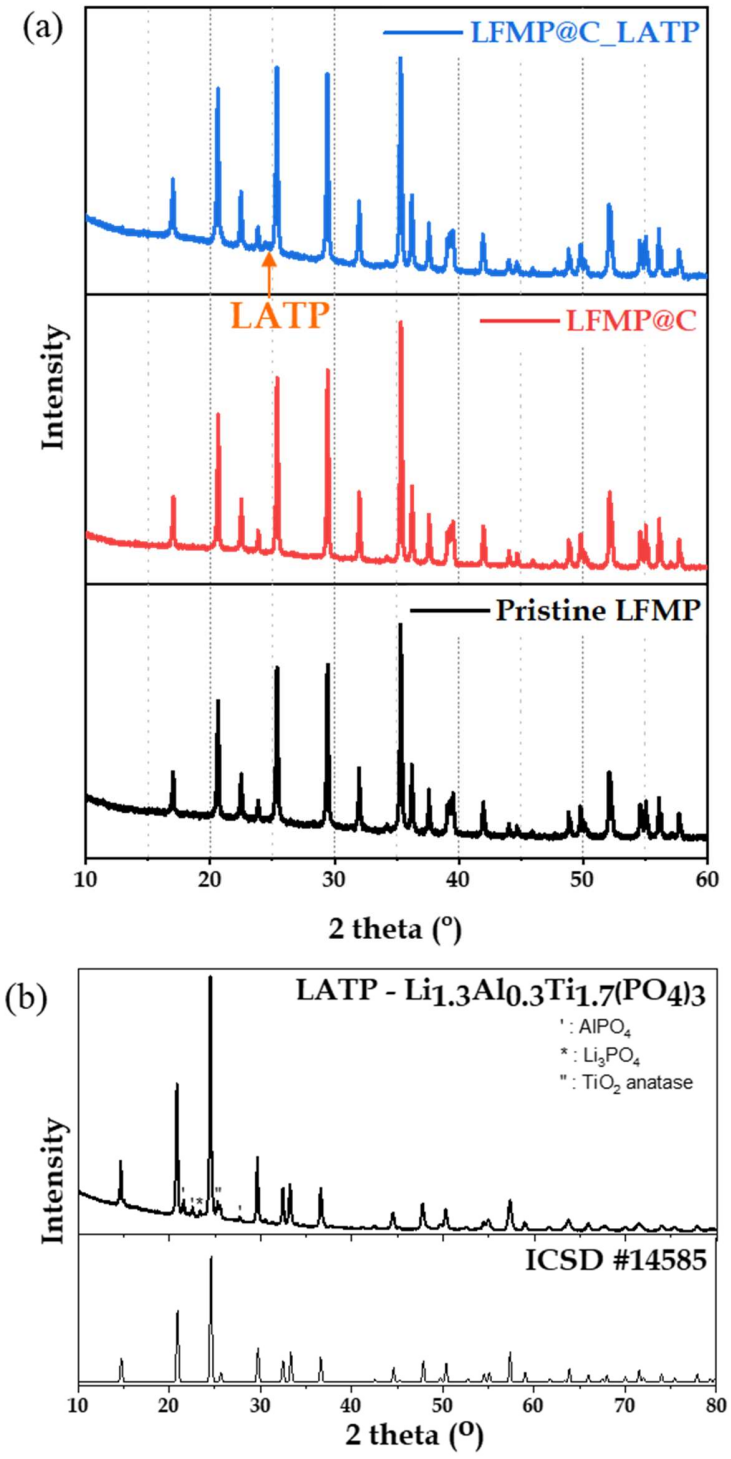

Fig 3.1 The XRD patterns of (a) pristine LFMP, LFMP@C, LFMP@C_LATP, and (b) LATP

synthesized at the same conditions.

3.1.2 ^{7}Li and ^{31}P magic angle spinning nuclear magnetic resonance

It is important to study the local environment of Li as it is involved in the electrochemical reactions of Li-ion batteries. In addition, the formation of LATP can be confirmed by the magic angle spinning (MAS) nuclear magnetic resonance (NMR) measurements since all related phases in the LFMP@C_LATP material are revealed as shown in **Fig. 3.2**. **Fig. 3.2(a)** shows the spectrum of ^{7}Li MAS measured at a spinning rate of 27 kHz for LFMP@C_LATP. A single isotropic peak observed at -1.2 ppm with large spinning sidebands confirms the presence of a single local Li-ion environment in octahedral sites, due to the interaction of the ^{7}Li nucleus with the unpaired electrons on the metal atom through the Li-O-M bond for $LiMPO_4$ (M = Fe, Mn, Co, Ni) and the dominant occupation of Li ions with six-fold oxygen coordination for LATP. For the synthesized LATP, an isotropic ^{7}Li peak at -18.5 ppm can be observed as shown in **Fig. 3.3(a)**.

Considering ^{31}P MAS NMR spectra of the LFMP@C_LATP (**Fig. 3.2(b) and (c)**), two peaks at 4879.2 and -28.5 ppm are recorded at a spinning rate of 12 KHz. It should be emphasized that the ^{31}P MAS NMR spectra are very sensitive to the chemical bonding of P with different neighboring atoms. The peak at 4879.2 ppm relates to the local environment of P in the olivine phosphate material while the peak at -28.5 ppm represents $P(OM)_4$, of the phosphate group of LATP, matching with the result observed for the synthesized LATP an isotropic ^{31}P peak at -26.5 ppm, **Fig. 3.3(b) and (c)**). The ^{31}P MAS NMR measurements further confirm the formation of LATP, supporting our previous XRD results. More importantly, the NMR measurements indicate the compatibility between the olivine LFMP and the LATP coating material. With the presence of LATP, Li ions can be easily transported within the LATP structure using interstitial sites connected

by low–energy barriers.[67,68] As a result, the Li-ion migration at the interfaces can be regulated, and the inferior Li-ion transfer kinetics of the olivine material can be mitigated.

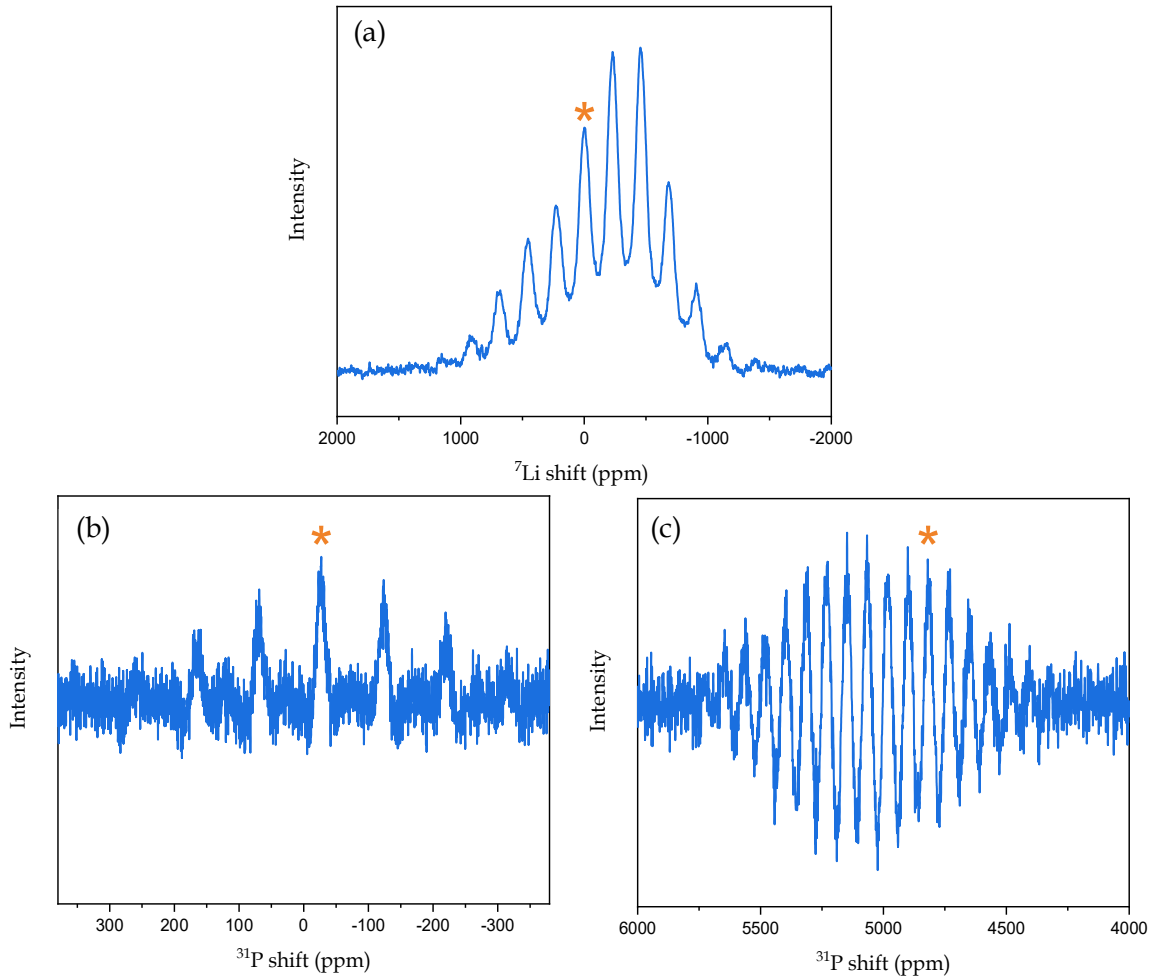

Fig. 3.2. (a) ^{7}Li, (b), and (c) ^{31}P MAS NMR spectra of LFMP@C_LATP. The isotropic peaks are marked with asterisks.

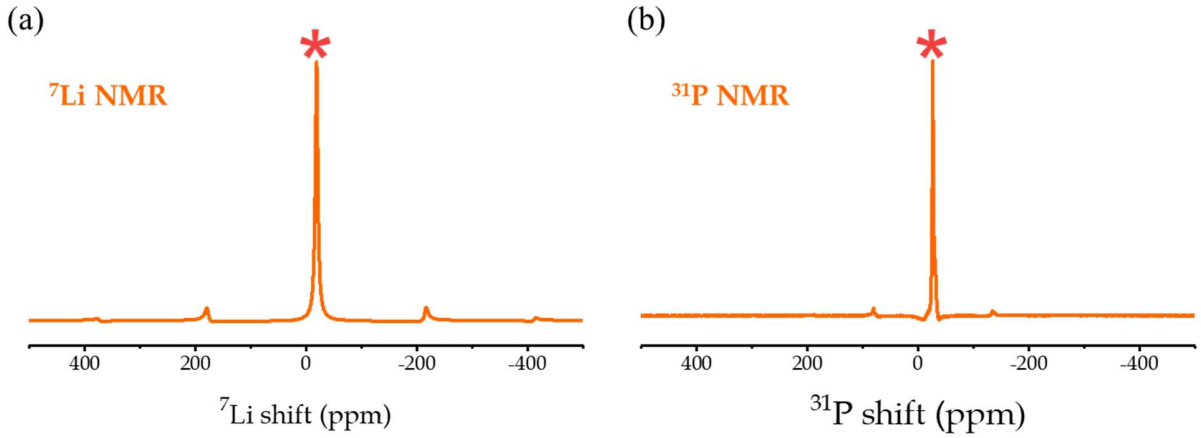

Fig. 3.3. (a) ^{7}Li and (b) ^{31}P MAS NMR spectra of LATP synthesized under the coating conditions. The isotropic peaks are marked with asterisks.

3.1.3 Raman spectroscopy and Thermal gravimetric analysis

Raman spectroscopy is the technique of choice for characterizing carbon-based materials used in Li-ion batteries. **Fig. 3.4(a)** shows the Raman spectra of LFMP@C and LFMP@C_LATP to investigate the nature of the carbon coating. Two prominent Raman peaks located at 1350 and 1594 cm^{-1} are observed, corresponding to D-band which is attributed to disordered carbon, and G-band which is attributed to graphitic carbon.[69] The observed I_D/I_G ratio is relatively high for both LFMP@C and LFMP@C_LATP, indicating the dominance of amorphous carbon coating.[70] These results are consistent with the XRD results where no peak of graphitic carbon can be clearly identified.

Fig. 3.4(b) shows the thermal gravimetric analysis (TGA) curves of LFMP@C and LFMP@C_LATP at a heating rate of 10 °C min^{-1} in the air from room temperature to 750 °C. The TGA results reveal a slight weight loss at low temperatures, corresponding to the release of materials absorbed on the particle surface. As the temperature increases, the weight gain obtained below 400°C may be due to the partial oxidation of M^{+2} to M^{+3} (M = Fe, Mn). The major weight loss due to carbon combustion can be observed when the loss exceeds the weight gain due to M^{2+} oxidation, and therefore, a fractional reduction consistent with M^{2+} oxidation must be taken into account to determine the actual content of the carbon coating.[71] Accurately distinguishing M^{2+} oxidation from carbon combustion is challenging. A final weight loss of approximately 2.15% is observed for LFMP@C while a loss of 2.84% is roughly calculated for LFMP@C_LATP. Even at relatively low levels, a conductive carbon coating layer is essential for conducting electrons through the entire surface of the olivine particles, thus improving the kinetics and reversibility of the Li insertion/extraction during charge/discharge processes.

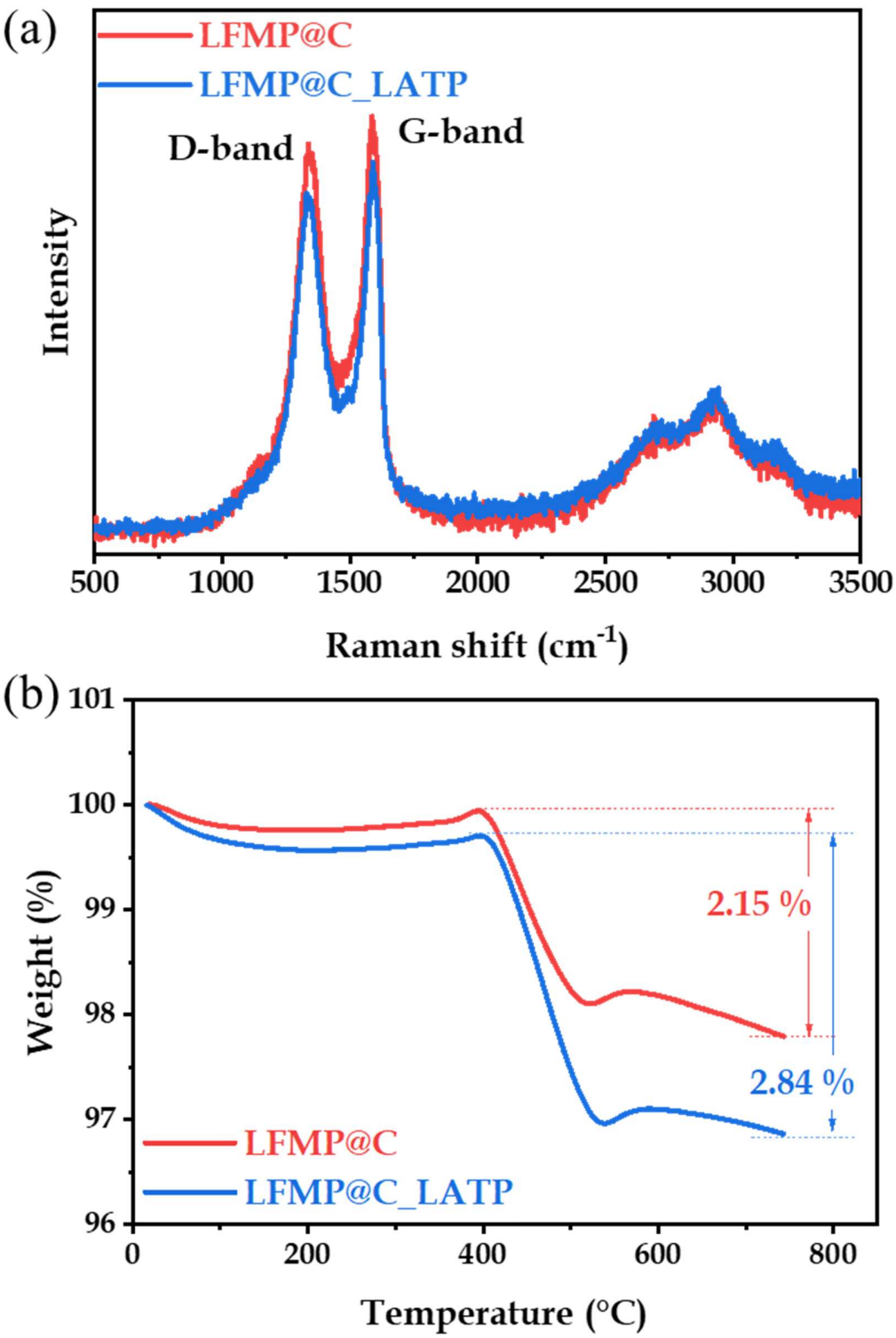

Fig. 3.4. (a) Raman spectra and (b) TGA curves of LFMP@C and LFMP@C_LATP.

3.1.4 Field emission scanning electron microscopy and energy dispersive x-ray spectroscopy

Fig. 3.5 shows the morphology and elemental distribution for Fe, Mn, Ti, and C in the LFMP@C_LATP. As shown in **Fig. 3.5(a)** the LFMP@C_LATP particles exist in an agglomerated form with a wide range of particle sizes as a result of the solid-state reaction, which has limitations in controlling particle nucleation, growth, and aggregation. The formation of solid solution olivine LFMP can be represented by the uniform distribution of Fe and Mn while the presence of Ti indicates the inhomogeneous distribution of LATP on the LFMP particles (**Fig. 3.5 (b-f)**). The Al signal is less intense compared to the Ti due to the lower elemental concentration of Al. The good distribution of C expresses the carbon coating on the LFMP material.

It should be emphasized that there are several challenges to homogeneously coating carbon and LATP on the LFMP particle surface. First, it is difficult to uniformly distribute solid precursors of carbon and LATP on the LFMP particle surface. Second, considering the heterogeneous nucleation, carbon and LATP can nucleate and grow at some favorable sites on the LFMP particle surface which have relatively lower surface energy. Consequently, the coating materials can exist locally, especially for LATP, as indicated by the significant agglomeration of Ti (**Fig. 3.5(e)**). In addition, some small-sized particles may acquire enough kinetic energy in the high-temperature process to migrate at the nanometer scale and sinter to become larger and more thermodynamically stable, which also affects the distribution of carbon and LATP on the LFMP particle surface.

Although it is challenging to achieve a homogeneous and thin coating throughout the material, the coating can provide channels for the transport of both electrons and Li-ions during cycling. The coating of carbon and LATP, even with a non-uniform structure, can be expected to efficiently regulate the surface reactions to improve the electrochemical performance of the LFMP material.

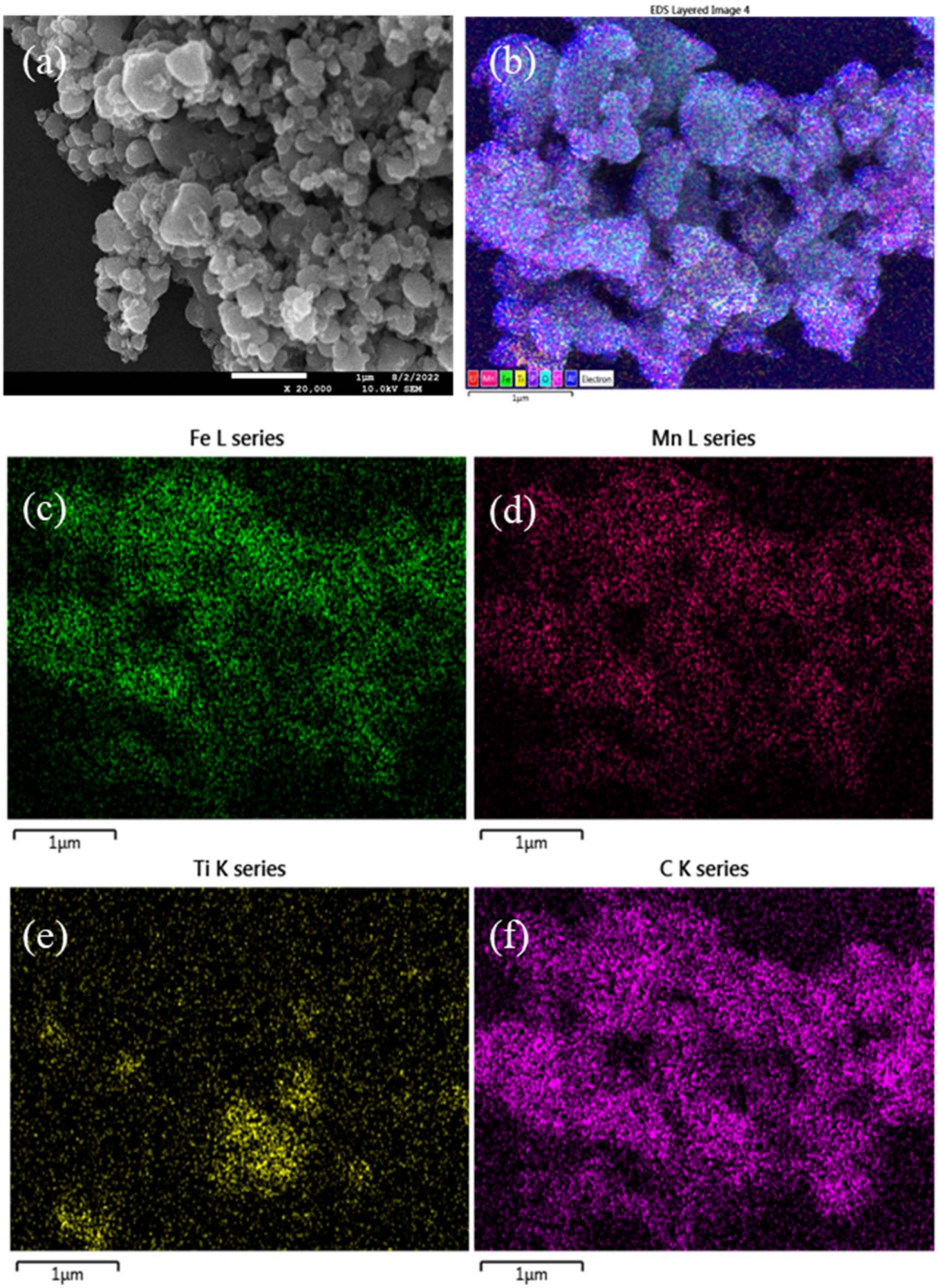

Fig. 3.5. (a) SEM image and (b) EDS image of LFMP@C_LATP with corresponding elemental distribution (c) Fe, (d) Mn, (e) Ti, and (f) C.

3.2 Electrochemical performance

3.2.1 Cyclic voltammetry

Cyclic voltammetry has long been a fundamental analytical technique to evaluate the oxidation and reduction potential as well as the reversibility of the redox reactions. **Fig. 3.6(a)** shows the CV profiles of pristine LFMP, LFMP@C, and LFMP@C_LATP at a rate of 100 mV sec^{-1} in the voltage range of 2.0-4.5V (vs. Li/Li^{+}). For all samples, the redox reactions of Fe^{2+}/Fe^{3+} exhibit an oxidation peak at ~ 3.58 V and a reduction peak at ~ 3.45 V while the redox reactions of Mn^{2+}/Mn^{3+} exhibit an oxidation peak at ~ 4.17 V and a reduction peak at ~ 3.91 V. Among those materials, only LFMP@C_LATP possesses additional reversible reduction and oxidation peaks at the low voltage region of 2.0-3.0 V (vs. Li/Li^{+}) as highlighted in **Fig. 3.6(a)**. The reversible peaks at the voltage region of 2.0-3.0 V can be attributed to the insertion/extraction of Li ions into/from the LATP component. To confirm that, the CV profile corresponding to the synthesized LATP material is measured and shown in **Fig. 3.6(b)**, exhibiting reversible redox couples in the low voltage range of 2.0-3.0 V (vs. Li/Li^{+}) due to the Li-ion intercalation in different LATP crystal sites.[72,73] It should be noted that the Ti^{4+} substitution by Al^{3+} and Li^{+} in the LATP structure generally leads to the Li-ion occupation at different sites: the well-known M1 sites with octahedral geometry and the vacant neighboring sites for charge compensation. The Li-ions can easily jump between the different sites in the LATP structure, making the LATP an excellent Li-ion conductor.[74,75] Once coated on the LFMP

particles, the Li-ion movement between the different sites in the LATP structure can possibly be induced by the inferior Li-ion diffusion in the core LFMP material, resulting in the appearance of multi-redox peaks in the active voltage range of LATP as shown in **Fig 3.6(a)**. As an electrochemical material, the electrochemical window of LATP merges with the LFMP material to extend the operating voltage range of the cathode material.

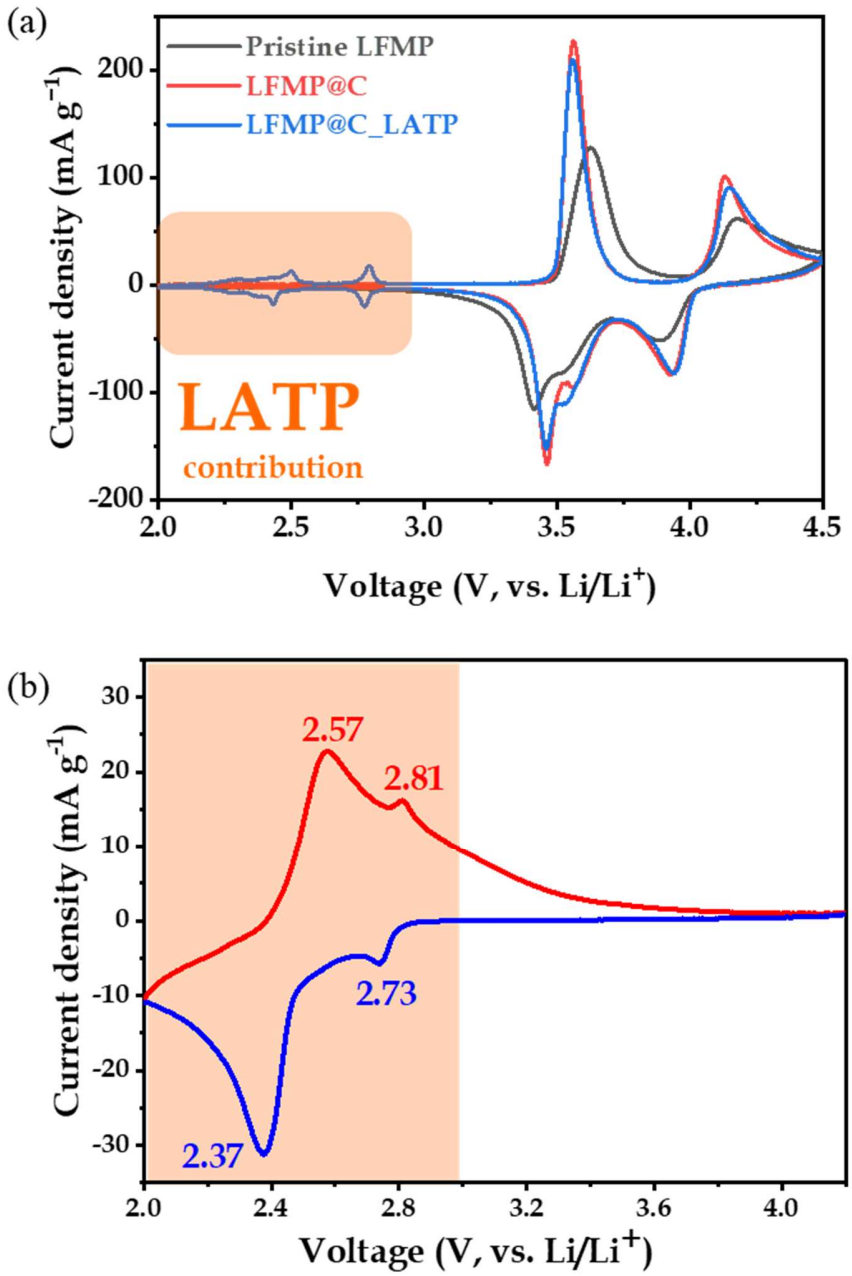

Fig. 3.6. (a) CV profiles of pristine LFMP, LFMP@C, and LFMP@C_LATP. (b) CV profile of LATP prepared under the conditions for coating.

3.2.2 Galvanostatic intermittent titration technique

Galvanostatic intermittent titration technique (GITT) is an experimental method to measure the change in open circuit voltage by applying a constant current to induce a change in voltage during charging and discharging, and then cutting off the current supply. Applying a constant current to the electrode material causes a Li-ion concentration gradient due to delithiation and lithiation from the electrode material particles.

Fig. 3.7(a) shows the GITT measurements for the LFMP@C and LFMP@C_LATP. Typical voltage vs. time plots in selected charge-rest and discharge-rest periods are given in **Fig. 3.7(b, c)**, showing the estimation of the quasi-equilibrium potential, the voltage difference after a charge or discharge pulse, and the voltage difference after relaxation. Two characteristic voltage plateaus around 3.5 and 4.1 V (vs. Li/Li^+), corresponding to the redox reactions of Fe^{2+}/Fe^{3+} and Mn^{2+}/Mn^{3+}, can be observed from the charge and discharge curves of both LFMP@C and LFMP@C_LATP. The LFMP@C_LATP generally achieves relatively longer and more stable plateaus with lower quasi-equilibrium potential during charging than the LFMP@C. The voltage differences after a charge or discharge pulse, and after relaxation are also smaller for the LFMP@C_LATP than for the LFMP@C (**Fig. 3.7(b, c)**), indicating that the capacity can be delivered more stably for the LFMP@C_LATP and a better structural adaptation of the material during cycling after coating with carbon and LATP. While the LFMP@C can deliver a charge capacity of 149.65 mAh g^{-1}, the LFMP@C_LATP can deliver a charge capacity of 164.69 mAh g^{-}

[1]. Considering the discharge, LFMP@C can deliver a capacity of 147.10 mAh g^{-1}, and the LFMP@C_LATP can deliver a better capacity of 156.28 mAh g^{-1}.

The remarkable improvement of LFMP@C_LATP over LFMP@C can be attributed to the presence of LATP coating. A combination of carbon and LATP coating takes advantage of both carbon and LATP to remarkably improve the electrochemical characteristics of the olivine cathode material. As shown in **Fig. 3.7(a)**, when carbon and LATP are coated simultaneously on the LFMP particles, the electrochemically activated onset voltage decreases for the LFMP@C_LATP. Consequently, Li-ions can be easily extracted from the LATP at the beginning of the charging at a relatively low voltage, forming a Li-ion concentration gradient between the surface (LATP) and the core (LFMP). The Li-ion concentration gradient then becomes the driving force for Li ions' continuous and consistent movement from the core LFMP material to the outer layer. Li ions occupy the empty spaces and then are rapidly extracted due to the high ion-conducting characteristic of LATP.

Regarding discharging, Li-ions first occupy the Li sites within the lithiated LATP. As a result, a Li-ion enriched zone is formed at the particle surface. After that, Li ions can easily migrate to neighboring vacancies and gradually move into the core lithiated LFMP material since the cationic vacancies are considered mobile charged species. At the end of discharge, the working voltage drops but is still adequate for LATP and thus causes the continuous lithiation of the LATP, providing an additional capacity to the cathode material.

Since the inferior Li transfer kinetics is mitigated, the LFMP@C_LATP material shows significantly larger charge and discharge plateaus, yielding higher capacities than conventional material with only carbon coating (LFMP@C). It should be noted that a detailed assessment of LATP's capacity contribution is challenging. LATP not only simply provides an additional capacity but also induces the charge transfer from the core LFMP. Nevertheless, the achievement of better capacity delivery and more excellent retention can be expected from the contribution of LATP.

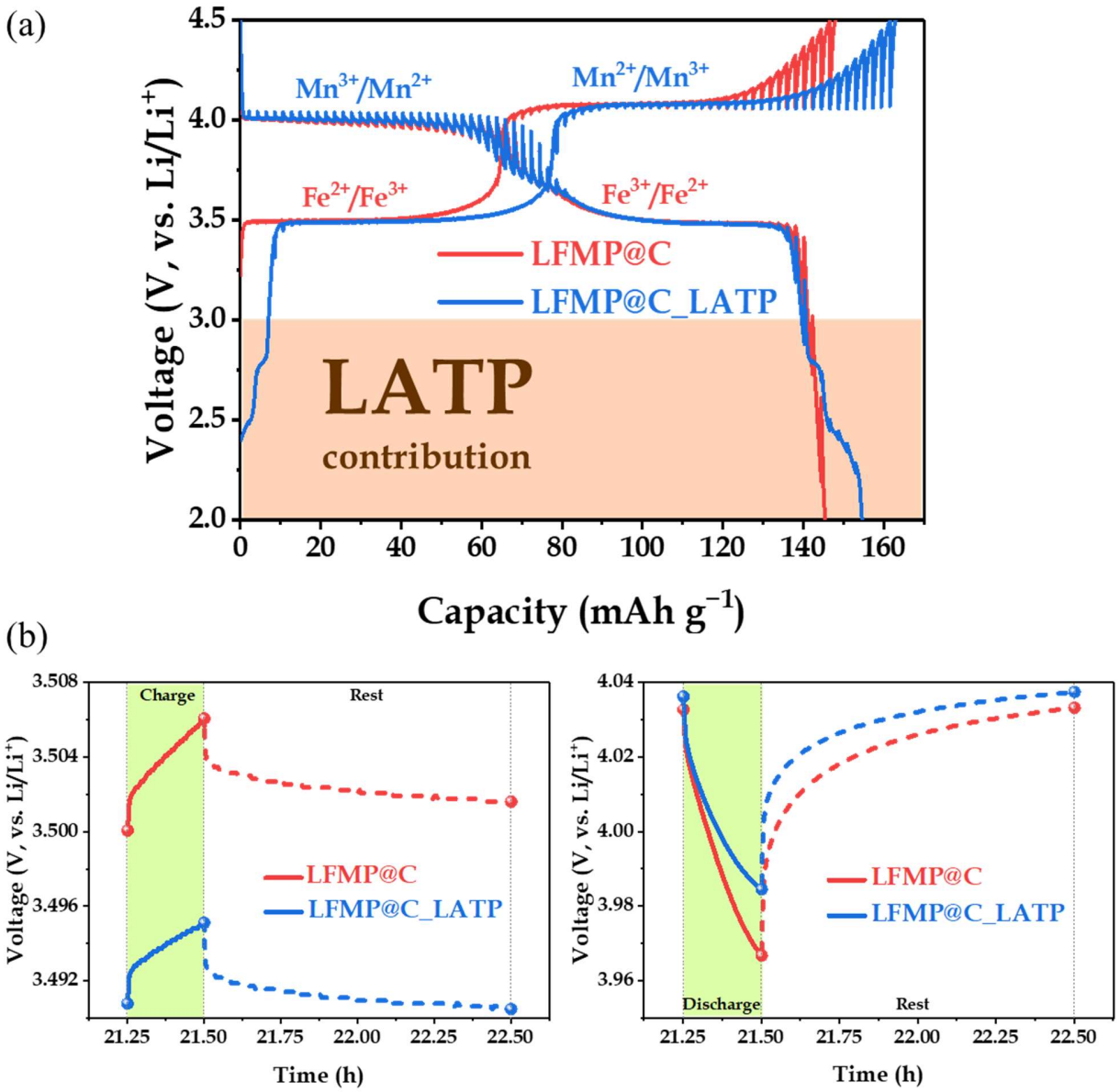

Fig. 3.7. (a) GITT profiles and (b) typical charge-rest and discharge-rest pulses of LFMP@C and LFMP@C_LATP. The cells are constantly charged or discharged at 0.05 C for 15 min, followed by relaxation for 1h in the voltage range of 2.0-4.5 V, vs. Li/Li^+.

3.2.3 Electrochemical impedance spectroscopy

Electrochemical impedance spectroscopy (EIS) is a powerful tool to investigate electrochemical kinetic reactions for the pristine LFMP, LFMP@C, and LFMP@C_LATP electrodes as shown in **Fig. 3.8**. As indicated in **Fig. 3.8(a)**, the Nyquist plots are composed of a semicircle at high to medium frequency related to the charge-transfer resistance (R_{ct}) and a linear part at a low-frequency range related to the Warburg impedance. Obviously, coating the pristine LFMP particles with either carbon (LFMP@C) or carbon and LATP (LFMP@C_LATP) helps reduce the R_{ct} of the electrode. A lower charge-transfer resistance is observed for the LFMP@C_LATP electrode compared to the LFMP@C electrode, indicating a better charge transfer throughout the LFMP@C_LATP electrode than the LFMP@C electrode.

In addition, the D_{Li}^{+} estimated from the EIS is reversibly proportional to the square of the Warburg factor (σ) ($D_{Li}^{+} \propto 1/\sigma^2$) based on the following equation:

$$D_{Li^+} = \frac{R^2T^2}{2A^2n^4F^4C^2\sigma^2}$$

where R is the gas constant, T is the absolute temperature, A is the surface area of the cathode electrode, n is the number of electrons per molecule during oxidation, F is the Faraday constant, C is the Li ion concentration, and σ is the Warburg factor.

As indicated in above equation, a smaller Warburg factor (σ) reflects a larger D_{Li}^{+} and thus a better Li-ion diffusion. The Warburg factor σ can be estimated based on the linear relationship between Re(Z) and $\omega^{-1/2}$ ($Re(Z) \propto \sigma\omega^{-1/2}$) as provided in **Fig. 3.8(b)**

and **Table 3.1**. Obviously, a smaller value of σ is obtained for the LFMP@C_LATP electrode compared to the LFMP@C and pristine LFMP electrodes, indicating a better D_{Li^+} in the LFMP@C_LATP electrode.

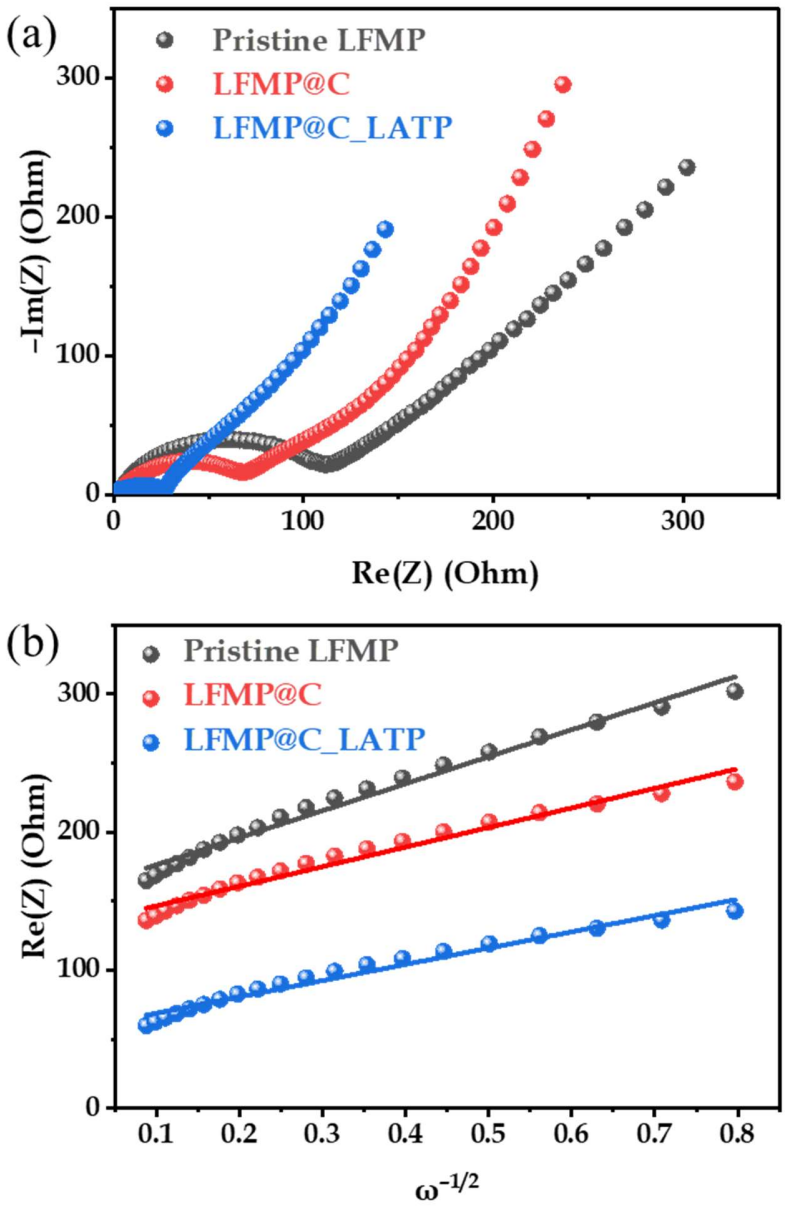

Fig. 3.8. (a) Nyquist plots and (b) the linear relationship between Re(Z) and $\omega^{-1/2}$ of pristine LFMP, LFMP@C and LFMP@C_LATP. The linear relationship is calculated in the low-frequency range of 100 mHz to 1 Hz.

Table 3.1. Slope and intercept of the relationship between the resistance (Re(Z)) and the inverse square root of the angular frequency ($\omega^{-1/2}$) of pristine LFMP, LFMP@C, and LFMP@C_LATP.

Equation	y = a.x + b		
Material	**Pristine LFMP**	**LFMP@C**	**LFMP@C_LATP**
Slope	**195.49 ± 5.79**	**141.79 ± 5.39**	**117.74 ± 4.79**
Intercept	156.99 ± 2.25	132.62 ± 2.10	57.31 ± 1.86

3.2.4 Cycling performance

Fig. 3.9 shows the rate performance of pristine LFMP, LFMP@C and LFMP@C_LATP with their typical performance at 0.05 C. **Table 3.2** summarizes their average discharge capacity at various C rates from 0.05 C to 5.0 C. A remarkable improvement can be observed for the olivine LFMP material after coating with carbon and LATP (LFMP@C_LATP), especially at high C rates. While the pristine LFMP can provide an average discharge capacity of 147.49 mAh g^{-1} at 0.05 C, an improvement can be achieved by carbon coating as an average discharge capacity of 155.76 mAh g^{-1} is delivered by the LFMP@C. A further improvement is obtained for the LFMP@C_LATP with an average discharge capacity of 158.15 mAh g^{-1} at the same current rate. The improvement becomes more prominent at hier current rates. At 1.0 C, an average discharge capacity of 134.47 mAh g^{-1} can be provided by the LFMP@C_LATP while the LFMP@C and the pristine LFMP can only provide an average discharge capacity of 126.35 and 108.87 mAh g^{-1}, respectively. Even at very high rate of 5.0 C, the LFMP@C_LATP can provide an excellent discharge capacity of about 103.35 mAh g^{-1} while the LFMP@C_LATP exhibits a discharge capacity of 95.05 mAh g^{-1} and the pristine LFMP shows a very poor capacity of 71.01 mAh g^{-1}.

As shown in **Fig. 3.9(b)**, several technical issues should be emphasized. First, the initial charge voltage is lower for the LFMP material with carbon and LATP coating (LFMP@C_LATP). Second, with the presence of LATP, additional charge and discharge

capacities at low voltage regions are observed for the LFMP@C_LATP. In addition, charge and discharge voltage plateaus of the LFMP@C_LATP material are more stable than those of the pristine LFMP and LFMP@C. These observations are consistent with the GITT measurement, revealing that the LATP coating crucially contributes its electrochemical properties and superior Li-ion conductivity to improve the performance of the core LFMP material.

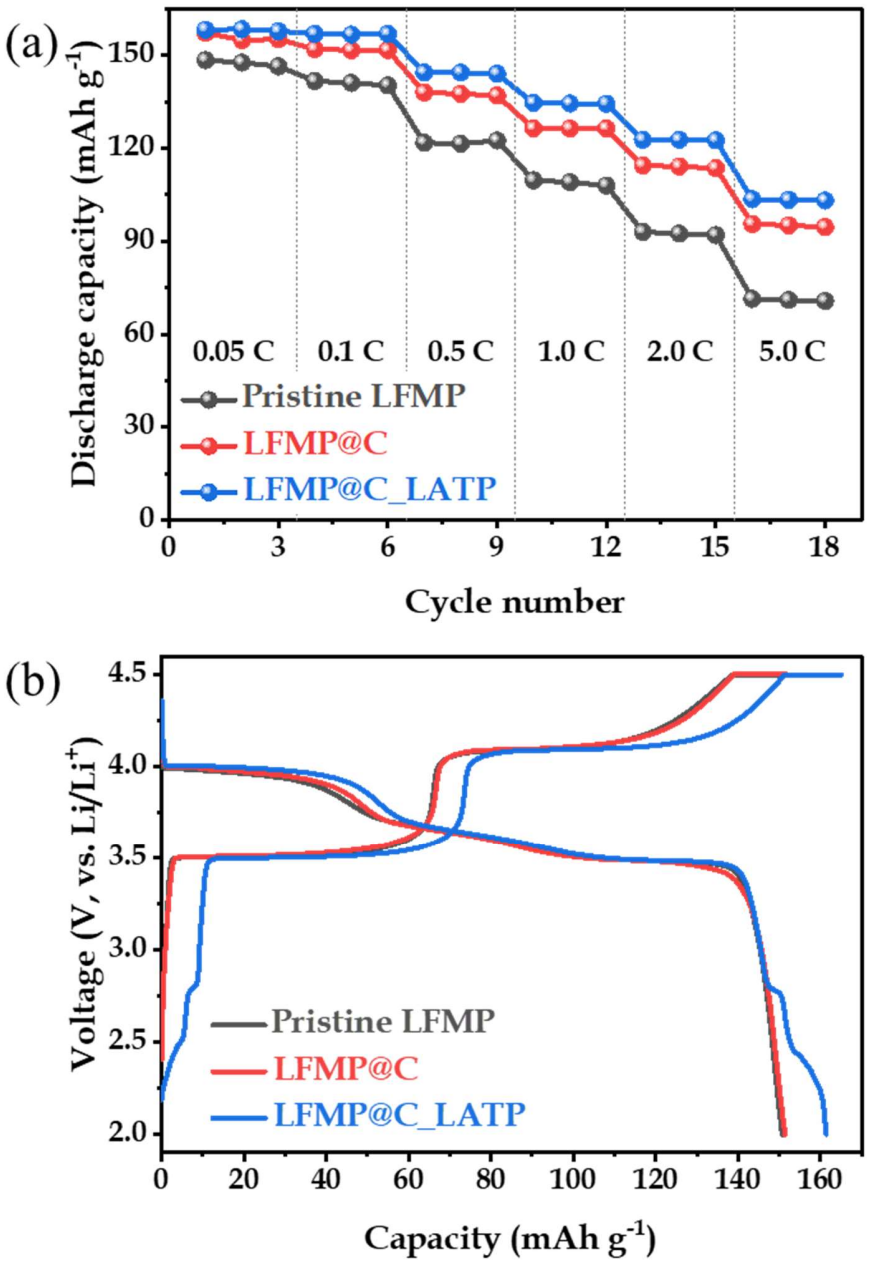

Fig. 3.9. (a) Rate performance at various C-rates from 0.05 C to 5.0 C and (b) typical charge-discharge profiles of pristine LFMP, LFMP@C and LFMP@C_LATP at 0.05 C.

Table. 3.2. The average discharge capacity corresponding to various C-rates (0.05 C to 5.0 C) of pristine LFMP, LFMP@C and LFMP@C_LATP.

Material	Average discharge capacity (mAh g^{-1})					
	0.05 C	0.1 C	0.5 C	1.0 C	2.0 C	5.0 C
Pristine LFMP	147.49	141.01	121.90	108.87	92.46	71.01
LFMP@C	155.76	151.78	137.50	126.35	114.01	95.05
LFMP@C_LATP	158.15	156.84	144.27	134.47	122.67	103.35

Superior capacity delivery and capacity retention of the LFMP@C_LATP to the pristine LFMP and LFMP@C can be observed by performing these materials at 1.0 C for 50 cycles as shown in **Fig. 3.10** and as summarized in **Table 3.3**. While the LFMP@C_LATP possesses discharge capacity of 131.68 and 125.46 mAh g^{-1} at the 1^{st} and 50^{th} cycles, respectively, giving a capacity retention of 95.3 %, the LFMP@C can deliver a discharge capacity of 120.27 mAh g^{-1} at the 1^{st} cycle and its discharge capacity reduces to 110.10 mAh g^{-1} at the 50^{th} cycle, giving a capacity retention of 91.5%. Of course, without coating, the pristine LFMP material exhibit the poorest performance with only 113.64 mAh g^{-1} can be delivered at the 1^{st} cycle. Discharge capacity of the pristine LFMP drastically reduces as obtaining 97.43 mAh g^{-1} after 50 cycles, giving a capacity retention of 85.7 %.

As demonstrated by previous GITT measurements, the LFMP@C_LATP shows a more stable operating voltage plateaus and a better structural adaption during cycling than the LFMP@C. At the electrode level, previous EIS measurements show a remarkable reduction in charge transfer resistance and significant improvement in Li-ion diffusion for the LFMP@C_LATP. Consequently, the LFMP@C_LATP exhibits a better capacity and capacity retention than both the pristine LFMP and LFMP@C. Thanks to the presence of LATP as an electrochemically active material and a Li-ion conductor on the LFMP particle surface, the redox reactions on the LFMP particle surface are regulated, resulting in mitigating the inferior Li transfer kinetics in the olivine LFMP material to practically

achieve a high-voltage cathode material for Li-ion batteries.

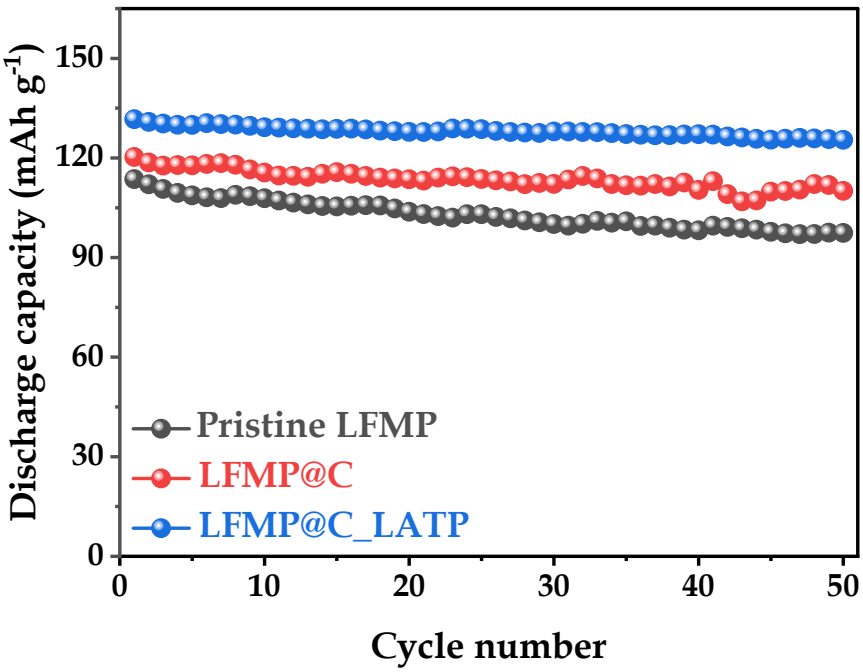

Fig. 3.10. Long cycle performance of pristine LFMP, LFMP@C, and LFMP@C_LATP at 1.0 C.

Table. 3.3. Summary of long cycle performance of pristine LFMP, LFMP@C, and LFMP@C_LATP at 1.0 C.

Material	Discharge capacity (mAh g^{-1})		Capacity retention (%)
	1st cycle	50th cycle	
Pristine LFMP	113.64	97.43	85.7
LFMP@C	120.27	110.10	91.5
LFMP@C_LATP	131.68	125.46	95.3

4. Conclusion

In this study, we have demonstrated that the construction of Li-ion and electron channels based on a simultaneous coating of carbon and $Li_{1.3}Al_{0.3}Ti_{1.7}(PO_4)_3$ (LATP) solid electrolyte on the surface of $LiFe_{0.4}Mn_{0.6}PO_4$ (LFMP) particles can effectively improve Li transfer kinetics, stabilize the operating voltage of the LFMP material for practical applications. Along with the carbon coating, which generally serves as a protective material and a conductive agent to improve electrical conductivity, the LATP component contributes several important factors as an electrochemically active material and a fast Li ion conductive compound. First, since the LATP is electrochemically active at a lower voltage than the LFMP material (2.0 V - 3.0 V, vs. Li/Li^+), the LATP coating can extend the operating voltage range of the product material. Second, the presence of LATP on the particle surface possible provides channels for Li-ion transport, thus improving Li diffusion. Third, LATP can initiate Li-ion extraction at a relatively low voltage during charging and regulate Li-ion insertion into the core material during discharging. Finally, LATP can self-store Li ions to contribute an extra capacity to the active material.

Our electrochemical investigation has revealed that the LFMP@C_LATP possesses a more stable operating voltage with a better structural adation during cycling. At the electrode scale, the LFMP@C_LATP electrode shows a lower charge transfer resistance and better Li-ion diffusion compared to the LFMP@C. As a result, the LFMP@C_LATP has superior performance compared to the pristine LFMP and conventional LFMP@C.

For instance, the LFMP@C_LATP can provide a discharge capacity of 158.3 mAh g^{-1} at 1.0 C with 95.3 % retention after 50 cycles while the LFMP@C and pristine LFMP can deliver 120.27 and 113.64 mAh g-1 with retention of 91.5 and 85.7% under the same cycling conditions. This coating approach can be universally applied for other active materials to achieve high energy, high rate, fast charge materials for Li-ion batteries.

5. References

1 EBIN, Burçak, et al. Recovery of industrial valuable metals from household battery waste. *Waste Management & Research*, 2019, 37.2: 168-175.

2 KIM, Tae-Hee, et al. The current move of lithium ion batteries towards the next phase. *Advanced Energy Materials*, 2012, 2.7: 860-872.

3 HORIBA, T., et al. Applications of high power density lithium ion batteries. *Journal of Power Sources*, 2005, 146.1-2: 107-110.

4 CHEN, Xiaopeng, et al. An overview of lithium-ion batteries for electric vehicles. In: *2012 10th International Power & Energy Conference (IPEC)*. IEEE, 2012. p. 230-235.

5 ARAVINDAN, Vanchiappan, et al. Lithium-ion conducting electrolyte salts for lithium batteries. *Chemistry–A European Journal*, 2011, 17.51: 14326-14346.

6 LEE, Hun, et al. A review of recent developments in membrane separators for rechargeable lithium-ion batteries. *Energy & Environmental Science*, 2014, 7.12: 3857-3886.

7 LEE, Hun, et al. A review of recent developments in membrane separators for rechargeable lithium-ion batteries. *Energy & Environmental Science*, 2014, 7.12: 3857-3886.

8 Fan, X., B. Liu, J. Liu, J. Ding, X. Han, Y. Deng, X. Lv, Y. Xie, B. Chen, and W. Hu, Transactions of Tianjin University, **2020**. 26(2): p. 92-103.

9 XU, Bo, et al. Recent progress in cathode materials research for advanced lithium ion batteries. *Materials Science and Engineering: R: Reports*, 2012, 73.5-6: 51-65.

10 WHITTINGHAM, M. Stanley. Lithium batteries and cathode materials. *Chemical reviews*, 2004, 104.10: 4271-4302.

11 XU, Gui-Liang, et al. Tuning the structure and property of nanostructured cathode materials of lithium ion and lithium sulfur batteries. *Journal of Materials Chemistry A*, 2014, 2.47: 19941-19962.

12 ZHOU, Shiyuan, et al. Crystal structural design of exposed planes: express channels, high-rate capability cathodes for lithium-ion batteries. *Nanoscale*, 2018, 10.37: 17435-17455.

13 CONG, Lina; XIE, Haiming; LI, Jinghong. Hierarchical structures based on two-dimensional nanomaterials for rechargeable lithium batteries. *Advanced Energy Materials*, 2017, 7.12: 1601906.

14 CHEN, Y.-H., et al. Porous cathode optimization for lithium cells: Ionic and electronic conductivity, capacity, and selection of materials. *Journal of Power Sources*, 2010, 195.9: 2851-2862.

15 ARORA, Pankaj; WHITE, Ralph E.; DOYLE, Marc. Capacity fade mechanisms and side reactions in lithium-ion batteries. *Journal of the Electrochemical Society*, 1998, 145.10: 3647.

16 NEWMAN, John, et al. Modeling of lithium-ion batteries. *Journal of power sources*, 2003, 119: 838-843.

17 ZHAO, Xiaohui, et al. Lithium/sulfur secondary batteries: a review. *Journal of Electrochemical Science and Technology*, 2016, 7.2: 97-114.

18 JULIEN, Christian M., et al. Comparative issues of cathode materials for Li-ion batteries. *Inorganics*, 2014, 2.1: 132-154.

19 MANTHIRAM, Arumugam. A reflection on lithium-ion battery cathode chemistry. *Nature communications*, 2020, 11.1: 1550

20 TUCCILLO, Mariarosaria, et al. Analysis of the phase stability of LiMO2 layered oxides (M= Co, Mn, Ni). *Crystals*, 2020, 10.6: 526.

21 CHEN, Xiaopeng, et al. An overview of lithium-ion batteries for electric vehicles. In: *2012 10th International Power & Energy Conference (IPEC)*. IEEE, 2012. p. 230-235.

22 MUNAKATA, F., et al. Chemical diffusion of Li+ ion in orthorhombic-LiMnO2. *Journal of materials science letters*, 2002, 21.2: 117-119..

23 XIA, Yu, et al. Designing principle for Ni-rich cathode materials with high energy density for practical applications. *Nano Energy*, 2018, 49: 434-452.

24 WANG, Bo, et al. Which of the nickel-rich NCM and NCA is structurally superior as a cathode material for lithium-ion batteries?. *Journal of Materials Chemistry A*, 2021, 9.23: 13540-13551..

25 BAKIERSKA, Monika, et al. Enhancing the lithium ion diffusivity in LiMn2O4− ySy cathode materials through potassium doping. *Solid State Ionics*, 2018, 317: 190-193.

26 ZHANG, Qi. Nanotechnology for Cathode Materials in Lithium-Ion Batteries. *Highlights in Science, Engineering and Technology*, 2023, 43: 333-339..

27 CAPSONI, Doretta, et al. Inhibition of Jahn–Teller cooperative distortion in LiMn 2 O 4 spinel by transition metal ion doping. *Physical Chemistry Chemical Physics*, 2001, 3.11: 2162-2166.

28 RAGAVENDRAN, K., et al. Jahn–Teller effect in LiMn 2 O 4: influence on charge ordering, magnetoresistance and battery performance. *Physical Chemistry Chemical Physics*, 2017, 19.3: 2073-2077..

29 MAUGER, Alain; JULIEN, Christian M. Olivine positive electrodes for Li-ion batteries: Status and perspectives. *Batteries*, 2018, 4.3: 39..

30 ZAGHIB, Karim; MAUGER, Alain; JULIEN, Christian M. Olivine-based cathode materials. In: *Rechargeable Batteries: Materials, Technologies and New Trends*. Cham: Springer International Publishing, 2015. p. 25-65..

31 XU, Yong-Nian; CHING, W. Y.; CHIANG, Yet-Ming. Comparative studies of the electronic structure of LiFePO 4, FePO 4, Li 3 PO 4, LiMnPO 4, LiCoPO 4, and LiNiPO 4. *Journal of applied physics*, 2004, 95.11: 6583-6585..

32 YAMADA, Atsuo; CHUNG, Sai-Cheong; HINOKUMA, Koichiro. Optimized LiFePO4 for lithium battery cathodes. *Journal of the electrochemical society*, 2001, 148.3: A224..

33 ZHANG, Miaomiao, et al. Etching preparation of (010)-defective LiFePO4 platelets to visualize the one-dimensional migration of Li+ ions. *The Journal of Physical Chemistry C*, 2015, 119.22: 12149-12156.

34 YAMADA, Atsuo; CHUNG, Sai-Cheong. Crystal Chemistry of the Olivine-Type Li (Mn y Fe1− y) PO 4 and (Mn y Fe1− y) PO 4 as Possible 4 V Cathode Materials for Lithium Batteries. *Journal of the Electrochemical Society*, 2001, 148.8: A960.

35 HWANG, Bing-Joe, et al. Template-free reverse micelle process for the synthesis of a rod-like LiFePO4/C composite cathode material for lithium batteries. *Journal of Power Sources*, 2009, 194.1: 515-519

36 YAMADA, Atsuo; CHUNG, Sai-Cheong; HINOKUMA, Koichiro. Optimized LiFePO4 for lithium battery cathodes. *Journal of the electrochemical society*, 2001, 148.3: A224.

37 ZHANG, Huanhuan, et al. A review of the doping modification of LiFePO4 as a cathode material for lithium ion batteries. *International Journal of Electrochemical Science*, 2020, 15.12: 12041-12067..

38 XU, Zhengrui, et al. recent developments in the doped LiFePO4 cathode materials for power lithium ion batteries. *Journal of the Electrochemical Society*, 2016, 163.13: A2600.

38 DOMINKO, Robert, et al. Impact of the carbon coating thickness on the electrochemical performance of LiFePO4/C composites. *Journal of the Electrochemical Society*, 2005, 152.3: A607..

40 CHO, Yung-Da; FEY, George Ting-Kuo; KAO, Hsien-Ming. The effect of carbon coating thickness on the capacity of LiFePO4/C composite cathodes. *Journal of Power Sources*, 2009, 189.1: 256-262.

41 CHO, Yung-Da; FEY, George Ting-Kuo; KAO, Hsien-Ming. The effect of carbon coating thickness on the capacity of LiFePO4/C composite cathodes. *Journal of Power Sources*, 2009, 189.1: 256-262.

42 LI, Zhaojin, et al. Controlled Hydrothermal/Solvothermal Synthesis of High-Performance LiFePO4 for Li-Ion Batteries. *Small Methods*, 2021, 5.6: 2100193.

43 CHUNG, Sung-Yoon; BLOKING, Jason T.; CHIANG, Yet-Ming. Electronically conductive phospho-olivines as lithium storage electrodes. *Nature materials*, 2002, 1.2: 123-128.

44 WANG, Yonggang; HE, Ping; ZHOU, Haoshen. Olivine LiFePO 4: development and future. *Energy & Environmental Science*, 2011, 4.3: 805-817.

45 WANG, Yuefang, et al. Mechanoactivation-assisted synthesis and electrochemical characterization of manganese lightly doped LiFePO4. *Journal of alloys and compounds*, 2010, 492.1-2: 675-680.

46 YOON, Won-Sub, et al. Electronic structural changes of the electrochemically delithiated LiFe0. 5Co0. 5PO4 cathode material studied by X-ray absorption spectroscopy. *Journal of Power Sources*, 2008, 183.1: 427-430.

47 NAM, Kyung-Wan, et al. In situ X-ray absorption and diffraction studies of carbon coated LiFe1/4Mn1/4Co1/4Ni1/4PO4 cathode during first charge. *Electrochemistry communications*, 2009, 11.4: 913-916. 43.

48 YAMADA, Atsuo; KUDO, Yoshihiro; LIU, Kuang-Yu. Reaction mechanism of the olivine-type Li x (Mn0. 6Fe0. 4) PO 4 (0⩽ x⩽ 1). *Journal of the Electrochemical Society*, 2001, 148.7: A747.

49 YAMADA, Atsuo; CHUNG, Sai-Cheong. Crystal Chemistry of the Olivine-Type Li (Mn y Fe1− y) PO 4 and (Mn y Fe1− y) PO 4 as Possible 4 V Cathode Materials for Lithium Batteries. *Journal of the Electrochemical Society*, 2001, 148.8: A960.

50 NEDOSEYKINA, Tatiana, et al. In situ X-ray absorption spectroscopic study for the electrochemical delithiation of a cathode LiFe0. 4Mn0. 6PO4 material. *Electrochimica Acta*, 2010, 55.28: 8876-8882., Proceedings of the National Academy of Sciences, **1983**. 80(16): p. 4945-4948.

51 YAMADA, Atsuo; CHUNG, Sai-Cheong. Crystal Chemistry of the Olivine-Type Li (Mn y Fe1− y) PO 4 and (Mn y Fe1− y) PO 4 as Possible 4 V Cathode Materials for Lithium Batteries. *Journal of the Electrochemical Society*, 2001, 148.8: A960.

52 ZHUANG, Hui, et al. Synergistic effect of composite carbon source and simple pre-calcining process on significantly enhanced electrochemical performance of porous LiFe0. 5Mn0. 5PO4/C agglomerations. *Electrochimica Acta*, 2019, 314: 102-114.

53 ZHOU, Xue, et al. A surfactant-assisted synthesis route for scalable preparation of high performance of LiFe0. 15Mn0. 85PO4/C cathode using bimetallic precursor. *Journal of Power Sources*, 2014, 265: 223-230..

54 SIN, Byung Cheol, et al. Enhanced electrochemical performance and manganese redox activity of LiFe0. 4Mn0. 6PO4 by iodine anion substitution as cathode material for Li-ion battery. *Journal of Power Sources*, 2016, 313: 112-119.

55 SIN, Byung Cheol, et al. Enhanced electrochemical performance of LiFe0. 4Mn0. 6 (PO4) 1− x (BO3) x as cathode material for lithium ion batteries. *Journal of Electroanalytical Chemistry*, 2015, 756: 56-60.

56 SIN, Byung Cheol, et al. Experimental and theoretical investigation of fluorine substituted LiFe0. 4Mn0. 6PO4 as cathode material for lithium rechargeable batteries. *Solid State Ionics*, 2014, 260: 2-7.

57 YANG, Chun-Chen; HUNG, Yen-Wei; LUE, Shingjiang Jessie. Improved electrochemical properties of LiFe0. 5Mn0. 5PO4/C composite materials via a surface coating process. *Journal of Power Sources*, 2016, 325: 565-574.

58 LI, Yuanchao, et al. Constructing a Hierarchical LiMn0. 8Fe0. 2PO4/C Cathode via Comodification of Li3PO4 and Graphite for High-Performance Lithium-Ion Batteries. *ACS Applied Energy Materials*, 2022, 5.9: 10983-10993.

59 VASSILIEV, Sergey Yu, et al. Electrochemical patterns of phase transforming intercalation materials: diagnostic criteria for the case of slow nucleation rate control. *Journal of The Electrochemical Society*, 2019, 166.6: A829.

60 IARCHUK, Anna R., et al. Influence of carbon coating on intercalation kinetics and transport properties of LiFePO4. *ChemElectroChem*, 2019, 6.19: 5090-5100.

61 NGUYEN, Dung The; KIM, Jimin; LEE, Youngil. A hybrid Carbon–Li1. 3Al0. 3Ti1. 7 (PO4) 3 conductive coating for high current rate LiFePO4 cathode material. *Chemical Engineering Journal*, 2023, 461: 141750.

62 GELLERT, Michael, et al. Compatibility study of oxide and olivine cathode materials with lithium aluminum titanium phosphate. *Ionics*, 2018, 24: 1001-1006.

63 XU, Qi, et al. Insights into the reactive sintering and separated specific grain/grain boundary conductivities of Li1. 3Al0. 3Ti1. 7 (PO4) 3. *Journal of Power Sources*, 2021, 492: 229631

64 XU, Qi, et al. Active Interphase Enables Stable Performance for an All-Phosphate-Based Composite Cathode in an All-Solid-State Battery. *Small*, 2022, 18.21: 2200266.

65 NISAR, Umair, et al. Valuation of surface coatings in high-energy density lithium-ion battery cathode materials. *Energy Storage Materials*, 2021, 38: 309-328.

66 KAUR, Gurbinder; GATES, Byron D. Surface Coatings for Cathodes in Lithium Ion Batteries: From Crystal Structures to Electrochemical Performance. *Journal of The Electrochemical Society*, 2022, 169.4: 043504.

67 EPP, Viktor, et al. Very fast bulk Li ion diffusivity in crystalline Li 1.5 Al 0.5 Ti 1.5 (PO 4) 3 as seen using NMR relaxometry. *Physical Chemistry Chemical Physics*, 2015, 17.48: 32115-32121.

68 MONCHAK, Mykhailo, et al. Lithium diffusion pathway in Li1. 3Al0. 3Ti1. 7 (PO4) 3 (LATP) superionic conductor. *Inorganic chemistry*, 2016, 55.6: 2941-2945.

69 YANG, Chun-Chen; HUNG, Yen-Wei; LUE, Shingjiang Jessie. Improved electrochemical properties of LiFe0. 5Mn0. 5PO4/C composite materials via a surface coating process. *Journal of Power Sources*, 2016, 325: 565-574.

70 DOEFF, Marca M., et al. Effect of surface carbon structure on the electrochemical performance of LiFePO4. *Electrochemical and solid-state letters*, 2003, 6.10: A207.

71 MINNETTI, Luca; MARANGON, Vittorio; HASSOUN, Jusef. Synthesis and characterization of a LiFe0. 6Mn0. 4PO4 olivine cathode for application in a new lithium polymer battery. *Advanced Sustainable Systems*, 2022, 6.5: 2100464.

72 AATIQ, Abderrahim, et al. On the structure of Li 3 Ti 2 (PO 4) 3. *Journal of Materials Chemistry*, 2002, 12.10: 2971-2978.

73 PATOUX, Sébastien; MASQUELIER, Christian. Lithium insertion into titanium phosphates, silicates, and sulfates. *Chemistry of Materials*, 2002, 14.12: 5057-5068.

74 REDHAMMER, G. J., et al. A single crystal X-ray and powder neutron diffraction study on NASICON-type Li1+ xAlxTi2− x (PO4) 3 (0≤ x≤ 0.5) crystals: Implications on ionic conductivity. *Solid state sciences*, 2016, 60: 99-107.

75 MONCHAK, Mykhailo, et al. Lithium diffusion pathway in Li1. 3Al0. 3Ti1. 7 (PO4) 3 (LATP) superionic conductor. *Inorganic chemistry*, 2016, 55.6: 2941-2945.